Arch Comput Methods Eng (2011) 18:315–340
DOI 10.1007/s11831-011-9062-9

# High-Resolution Finite Volume Methods on Unstructured Grids for Turbulence and Aeroacoustics

**Xesús Nogueira · Sofiane Khelladi · Ignasi Colominas · Luis Cueto-Felgueroso · José París · Héctor Gómez**

Published online: 27 July 2011


**Abstract** In this paper we focus on the application of a higher-order finite volume method for the resolution of Computational Aeroacoustics problems. In particular, we present the application of a finite volume method based in Moving Least Squares approximations in the context of a hybrid approach for low Mach number flows. In this case, the acoustic and aerodynamic fields can be computed separately. We focus on two kinds of computations: turbulent flow and aeroacoustics in complex geometries. Both fields require very accurate methods to capture the fine features of the flow, small scales in the case of turbulent flows and very low-amplitude acoustic waves in the case of aeroacoustics. On the other hand, the use of unstructured grids is interesting for real engineering applications, but unfortunately, the accuracy and efficiency of the numerical methods developed for unstructured grids is far to reach the performance of those methods developed for structured grids. In this context, we propose the FV-MLS method as a tool for accurate CAA computations on unstructured grids.

X. Nogueira (✉) · I. Colominas · J. París · H. Gómez
Departamento de Métodos Matemáticos y de Representación, Universidade da Coruña, A Coruña, Spain
e-mail: xnogueira@udc.es

S. Khelladi
Laboratoire de Dynamique des Fluides (DynFluid Lab.), Arts et Métiers ParisTech, Paris, France

L. Cueto-Felgueroso
Dept. of Civil and Environmental Engineering, Massachusetts Institute of Technology, 77 Massachusetts Ave., Cambridge, MA 02139, USA

## 1 Introduction

Computational Fluid Dynamics (CFD) has become an indispensable tool in both, design and research. In aerospace industry, it is difficult to find a project in which CFD is not present. However, and despite the great success that CFD has achieved, it is fair to acknowledge that it still has a long way to go. In turbulent flows, for example, the Reynolds number achieved in full-scale numerical simulations of flows is still very low, and it is very far from the numbers of interest in industrial processes. Even with this limitation, *Direct Numerical Simulation* (DNS) plays a key role in fundamental research. CFD has contributed to the advance in knowledge about turbulence, astrophysical processes and in general in those phenomena where experimental measurement is difficult or even impossible. Moreover, in these "virtual experiments", the researcher can access to every variable of interest. This kind of research has also favored the development of *turbulence models* that allow the computation of flows with higher Reynolds numbers (but at the expense of a lower accuracy). In this context it is worth mentioning the idea of *Large Eddy Simulation* (LES), in which the biggest scales of the flow are directly solved (that is, without any model) whereas the smaller flow scales are modeled.

Godunov's theorem [1] establishes that it is impossible to develop a monotone *linear* numerical scheme with an order of accuracy higher than one. That is, high-accuracy and the absence of new extrema near sharp gradients are two contradictory requirements for linear methods. This is the difficulty that high-order methods have to face. However, in CFD there is really a need of high-accuracy methods for problems in which is essential to capture the fine features of the flow. Thus, in the simulation of turbulent flows (both in DNS and LES) it is required a high *resolution* of the frequency spectrum. In DNS, for example, the amplitude of Fourier modes

of the velocity field is distributed continuously in a wide range of wave numbers. On the other hand, if the numerical scheme is not able to solve accurately the scales lying on the higher frequency range of the spectrum, the distribution of the energy spectrum is displaced to the high-frequency range and the simulation fails (*pile-up*).

Aeroacoustics is another field in which the accuracy requirements of the numerical method are critical. The low-amplitude of acoustic waves and the wide range of frequencies present in the solution makes very difficult the numerical resolution of these problems. The most usual approach to solve Computational Aeroacoustics (CAA) problems nowadays is the so-called "hybrid approach". In particular, when the Mach number is small, it is possible to separate the aerodynamic and acoustic problems. Thus, acoustic sources are obtained by a computation of the turbulent flow and propagated using a wave equation, the linearized Euler equations or other approaches.

In a hybrid approach, numerical methods with high-resolution are required to solve the turbulent flow and also the propagation of the acoustic sources. Moreover it is needed an adequate dissipation, and the requirements of the dissipation properties of the numerical scheme are different for the resolution of a turbulent flow or an acoustic problem. In this context, "high-resolution" means high accuracy in the Fourier space, that is, accuracy in the widest possible range of *frequencies*. Thus, even though "higher-order" usually is identified with "more accurate solution", it is possible the existence of more efficient procedures to increase the width of the range of frequencies solved than raising the order of the numerical scheme. In this context "adequate dissipation" means that the dissipation of the numerical scheme has to be enough to stabilize the computations without modifying the features of the flow (in turbulent computations) or dissipate the acoustic waves (in CAA computations). For example, quasi-spectral finite differences schemes [2–5] are commonly used in such high-accuracy demanding applications. In these schemes, some of the order that it could be possible to achieve is sacrificed to obtain a better approximation in a wider range of the frequency spectrum. These methods are very accurate and efficient, but unfortunately they require an structured grid to be applied. For rather complex geometries, however, different strategies have to be used. For example, the use of multi-block grids allows the use of structured grid procedures, but it requires an additional effort to build the grids and their interfaces. On the other hand, the global nature of classical spectral methods may be changed for a more local approach, following the spirit of *hp* finite element methods [6, 7]. Thus, the use of unstructured-grid methods is an attractive option. But this kind of methods presents several problems for its application to real engineering problems. Some of them suffer a great increase of the computational resources and many others have difficulties for the evaluation of high-order derivatives of the variables. Another approach that holds promise for the resolution of CFD problems on complex geometries is the so-called Isogeometric Analysis [8, 9]. This technology includes Finite Element Analysis as a special case, but also offers other possibilities, such as, for example, precise geometrical modeling or simplified mesh refinement. The main idea of Isogeometric Analysis is using Non-Uniform Rational B-Splines (NURBS) [10] as basis functions in a variational formulation. The use of NURBS leads to more robust [11] higher-order formulations and to enhanced spectral resolution of the approximation [12] compared to classical polynomial-based Finite Elements. We feel that the reason for this lies in two properties of NURBS not possessed by classical Finite Elements, namely, smoothness and non-interpolatory character. The basis functions built with the formulation employed in this paper do exhibit the smoothness and non-interpolatory character of NURBS and we believe that this fact may contribute to explain the robustness of our method.

Most Numerical schemes developed for unstructured grids are based on polynomial approximations. In this context, it is not easy to find other ways to improve the accuracy different from increasing the order of the numerical scheme.

When we use high-resolution schemes to solve compressible flows, an additional difficulty appears: the possible presence of shock waves. When using high-order schemes, a shock wave originates first-order errors that propagate through the domain of computation, far of the shock region. In order to deal with shock waves, and "circumvent" the Godunov's theorem high-order methods add some kind of numerical dissipation. This fact limits the resolution of the scheme, since small-scale features of the flow are damped out by this additional dissipation.

Among the most successful higher-order numerical schemes for unstructured grids we can cite higher-order finite volume methods [13–23], Discontinuous Galerkin methods [24–38], essentially non-oscillatory (ENO and WENO) methods [39–53], the Spectral Finite volume method [54–60] and Residual Distribution schemes [61–79].

These methods are designed in origin for the resolution of hyperbolic conservation laws, and their application to non-strictly hyperbolic equations is not straightforward. Thus, the discretization of viscous terms (of elliptic nature) in the Navier-Stokes equations is a source of problems. In fact, most of the differences between the Discontinuous Galerkin schemes for this set of equations relies in the discretization of viscous terms, and it is one of the main drawbacks of these numerical schemes.

On the other hand, the Discontinuous Galerkin method obtains very accurate results in the case of purely hyperbolic systems when the flow is smooth. However, the use

of this numerical scheme when shock waves are present is difficult. The spectral volume method, presents advantages in this case, since it is possible to apply the limiting techniques developed for finite volume methods. When dealing with shocks, ENO and WENO are the reference methods. They circumvent the Godunov's theorem by using nonlinear (data dependent) reconstructions. The idea is to use an adaptive stencil, looking for the stencil that obtains the less oscillatory solution. Originally developed for structured grids, the extension to unstructured grids is not straightforward due to the increase in the size of the stencils. Thus, only recently a modified WENO method has been applied to three-dimensional problems [49].

Nowadays, the use of finite volume methods with slope limiters is the most common approach to deal with compressible flows in engineering applications.

A high order method well-suited for the application on unstructured grids has been recently presented in [80, 81]. This method is based on the application of a meshfree technique (Moving LeastSquares) [82–84] in a finite volume framework. We refer to this numerical scheme as the FV-MLS method. One of its advantages is the increase of the order of accuracy without raising the number of degrees of freedom. Another interesting feature is the treatment of viscous terms in the Navier-Stokes equations, since viscous terms are directly computed at integration points. This procedure leads to a clear and accurate approximation of the viscous fluxes [85]. Moreover, since the FV-MLS method is a finite volume solver, it is possible to use any of the robust and widely used shock capturing techniques developed for the finite volume method. In order to improve the behavior of these shock-capturing methods, new selective limiting techniques have been proposed [86, 87]. In this paper we are going to focus on the application of the FV-MLS method to the resolution of CAA problems in a context of a hybrid approach. Thus, we examine here the ability of this numerical scheme to simulate turbulent compressible flows and also to solve the Linearized Euler equations.

The outline of this paper is as follows: In Sect. 2 we present a non-extensive review about the most common approaches to simulate compressible turbulent flows. Section 3 is devoted to present different techniques for the resolution of aeroacoustic problems, focusing on the different hybrid approaches. In Sect. 4 we review the FV-MLS method and point out several issues concerning the multiresolution properties of the numerical discretization and its application to the resolution of turbulent flows and aeroacoustics problems. In Sect. 5 we present a implicit turbulence model based on the multiresolution properties of the FV-MLS scheme. In Sect. 6 several numerical examples of the application of the FV-MLS method to aeroacoustics are exposed. Finally, we present the conclusions.

## 2 The Numerical Simulation of Turbulent Flows

The simulation of turbulence is one of the most challenging problems that the research community has to face nowadays. This is true not only from a "numerical" point of view, but also from more deeper sights. Thus, even the question about the nature of turbulence remains unclear [88]. However, although there is not a single definition of turbulence, it is possible to identify a number of common properties to every turbulent flow:

1. *Apparently* random and chaotic behavior.
2. Dependence on initial conditions.
3. A wide range of length and time scales.
4. Three-dimensional, time-dependent and rotational character.
5. Time and space intermittency.
6. Diffusion and dissipation phenomena.

Since the problem of the simulation of turbulence is vast enough to cover several books (for example [89–92]), our intention here is to present the most common approaches for the simulation of turbulent flows.

### 2.1 The Energy Cascade

The wide range of scales present in a turbulent flow suggested to Richardson [93] the idea of the self-similarity of turbulent flows. Then Kolmogorov [94] introduced the concept of *energy cascade*. Most of the kinetic energy of a turbulent flow is in the biggest vortices (biggest scales). These vortices are created by instabilities of the mean flow and they are also under the action of inertial instabilities that may break them down into smaller ones. These smaller vortices are also under the action of instabilities and they may break again. Each time that a vortex breaks the energy of the bigger scales is transferred to the smaller structures. This process is continuously taking place in a flow. Inertial forces dominate the process and viscosity does not take part in it. However, from a certain size of the smaller scales, the Reynolds number ($Re$) takes a value near to one. In this moment, viscous forces are not negligible and dissipation becomes important. The scale for which $Re \approx 1$ is called the *Kolmogorov scale*. Smaller vortices should be in a state in which the rate of kinetic energy received from larger vortices equals the rate of energy dissipated as heat by viscous forces. This hypothesis was introduced by Kolmogorov [94] and is known as the universal equilibrium theory.

With this theory and using dimensional analysis, it is possible to determine the size of the smaller structures in a turbulent flow [95]:

$$\eta \sim l Re_T^{\frac{-3}{4}} \tag{1}$$

$$v \sim u Re_T^{\frac{-1}{4}} \tag{2}$$

where $l$ is the typical size of bigger structures, $\eta$ is the typical size of the smaller vortices, $u$ is the typical velocity of bigger vortices and $v$ is the velocity of the smaller ones. Turbulent Reynolds number is given by $Re_T = k^{1/2} l/\nu$. $k$ is the kinetic energy of turbulent fluctuations per unit mass and $\nu$ is the kinematic molecular viscosity. We note that when the Reynolds number is increased, the size of the smaller scales decrease.

### 2.2 Length and Time Scales

One of the typical features of turbulent flows is the presence of a large number of structures with a very wide range of time and length scales. In the study of turbulence, there are four main sets of scales:

1. Large scale, based on the geometry ($l$).
2. Integral scale, it is a fraction (usually 20%) of the large scale.
3. Taylor microscale ($\lambda$).
4. Kolmogorov scale ($\eta$).

Using dimensional analysis and assuming Kolmogorov's universal equilibrium theory, it is concluded that the dynamics of the smaller scales will depend on the kinetic energy dissipation rate per unit of mass $\epsilon$ ($[L^2T^{-3}]$) and on the kinematic viscosity $\nu$ ($[L^2T^{-1}]$). Thus, considering that $\epsilon$ and $\nu$ as the dimensional parameters we obtain length, time and velocity Kolmogorov's scales:

$$\eta \equiv (\nu^3/\epsilon)^{\frac{1}{4}} \tag{3}$$

$$\tau \equiv (\nu/\epsilon)^{\frac{1}{2}} \tag{4}$$

$$v \equiv (\nu\epsilon)^{\frac{1}{4}} \tag{5}$$

From this expressions it is possible to obtain the expression for $v$ given by (2).

The Taylor microscale for isotropic turbulence verifies $\lambda \sim (l\eta^2)^{\frac{1}{3}}$. Moreover, the *eddy turnover time* is a measure of the time that a vortex needs to interact with its surroundings. It is defined as a characteristic time in terms of a characteristic length ($l$) and a characteristic velocity ($k^{1/2}$).

An important consideration is the spectral representation of the properties of a turbulent flow. As turbulent flows contain a continuous spectrum of scales, it is convenient to perform an analysis in terms of spectral distribution of energy. Thus, the energy spectrum ($E(\kappa)$) is represented as the decomposition in wavenumbers ($\kappa$). In general, the distribution of energy is a function of $\nu$, $\epsilon$, l, $\kappa$ and the mean strain rate $S$. However, Kolmogorov suggests that there is a range of scales for which the energy transferred by inertial effects is dominant, and then the spectral distribution of energy only depends on $\epsilon$ and $\kappa$. This range of scales is the inertial subrange.

### 2.3 Direct Numerical Simulation and Statistically Averaged Methods

The most straightforward approach for the simulation of a turbulent flow is to solve the full range of scales in the Navier-Stokes equations. Unfortunately, the number of flows we can compute with this approach is very limited. The higher the Reynolds number is, the smaller the size of the scales present in the flow. In fact, it can be proven [92] that the ratio of the largest to the smallest flow scale is proportional to $Re^{9/4}$. This proportion suggest that the number of nodes scales with $Re^{9/4}$. This implies prohibitively computer requirements with current technology for most flows of engineering interest. However, DNS plays a very important role in fundamental research [96]. Thus, the extensive use of direct simulations has been crucial for a better knowledge of turbulence and for the development of models that allow the simulation of flows at higher Reynolds numbers.

Although the direct solution of the Navier-Stokes equations is not applicable to most engineering problems, there is still a need for solving them in real practical applications. Thus, a great effort has been devoted to developing models to simulate the effect of the unresolved scales. Probably, the most common approach in flows of engineering interest has been the use of the *statistical time averaging* of the solution. This technique, called the Reynolds averaged numerical simulation (RANS) is based on the idea of the decomposition of the flow in two parts: The statistical average and a fluctuation:

$$u_i = \overline{u}_i + u_i' \tag{6}$$

The averaging process reduces the number of scales in the solution, but also precludes the numerical scheme from capturing the fine features of the flow. Thus, the effect of small scales (the fluctuation) is included by a turbulent model.

The RANS equations for an incompressible flow are the following [92]:

$$\begin{aligned} &\frac{\partial \overline{u}_i}{\partial x_i} = 0 \\ &\rho \frac{\partial \overline{u}_i}{\partial t} + \rho \overline{u}_j \frac{\partial \overline{u}_i}{\partial x_j} = -\frac{\partial p}{\partial x_i} + \frac{\partial (2\mu S_{ij} - \rho \overline{u_j' u_i'})}{\partial x_j} \end{aligned} \tag{7}$$

the superindex $\bar{}$ means an statistical average of the variable, and repeated indices indicate summation (Einstein notation). The term $\rho \overline{u_j' u_i'}$ appears due to the non-linearity of the Navier-Stokes equations. It is known as the Reynolds stress tensor (or turbulent stress tensor). It introduces six additional unknowns to the system. In order to solve the system, we need to obtain additional equations relating the fluctuating part with the averaged part of the flow. The lack

of these equations is the *turbulent closure problem*. The attempts to find such relations represent the history of the evolution of turbulent models.

The first attempts to develop a mathematical description of the Reynolds stress tensor were made by analogy with the molecular diffusion. Thus, Boussinesq introduces the concept of *turbulent viscosity* as the "turbulent" analog of molecular viscosity. As the viscous stress tensor is related to the velocity gradient by the molecular viscosity, the Boussinesq hypothesis relates turbulent stresses with the gradient of the averaged velocity by means of the turbulent viscosity. However, unlike molecular viscosity, which is independent of the flow, the turbulent viscosity is different for each flow. This dependence is the reason for the lack of an universal turbulent model.

The similarity between turbulence and molecular processes is also present in the Prandtl's theory of mixing length. He suggested that the turbulent viscosity can be defined from the so-called "mixing length", in an analogy with the kinetic theory of gases, that predicts the value of the molecular viscosity from the value of the molecular mean free path. Even though this hypothesis presents many theoretical problems to be justified [92], it works reasonably well in shear flows, when the right value of the mixing length is used. The idea of the mixing length is the basis of the so-called *algebraic models*.

The search of an universal turbulence model continued with models in which the turbulent viscosity is not only a function of the mixing length but also of other parameters. These additional parameters try to consider the "history" of the flow, in an effort to obtain a more realistic description of the Reynolds stresses. This is the origin of the $n-$equation models. These models introduce a new set of $n$ transport differential equations in addition to the conservation of mass, momentum and energy equations. Kolmogorov [97] was the first to propose a two-equation model. Since then, several sets of equations have been developed. Among others we can mention the $k-\epsilon$ model [98], the $k-\omega$ model [99], the SST model [100], or the $v^2-f$ model [101]. Several authors use the renormalization group theory to derive expressions for the turbulent viscosity [102, 103]. This modification improves the behavior of the turbulence models near the walls.

Algebraic and $n$-equation methods are widely used for real engineering applications. However, they have some drawbacks that preclude their use when high accuracy is required. RANS methods obtain acceptable results for statistically steady flows, which roughly means that all statistical properties are constant in time. This is not the case, for example, in phenomena such as transition, boundary layer separation or vortex interaction. Moreover they are unable to accurately predict turbulent flows at high Mach numbers [104]. The reason is the even more complex phenomena involved in turbulent compressible flows [105].

With the aim of showing the increase in difficulty, we apply the Reynolds averaging to the compressible Navier-Stokes equations. It is convenient to introduce the Favre averaging:

$$\widetilde{\Phi} = \frac{\overline{\rho\Phi}}{\overline{\rho}} \tag{8}$$

and

$$\Phi_i = \widetilde{\Phi}_i + \Phi_i'' \tag{9}$$

Thus, the Favre-averaged Navier-Stokes equations are:

$$\begin{aligned}
&\frac{\partial\overline{\rho}}{\partial t} + \frac{\partial[\overline{\rho}\widetilde{u}_i]}{\partial x_i} = 0\\
&\frac{\partial(\overline{\rho}\widetilde{u}_i)}{\partial t} + \frac{\partial[\overline{\rho}\widetilde{u}_i\widetilde{u}_j + \overline{p}\delta_{ij} + \overline{\rho u_i'' u_j''} - \overline{\tau_{ji}}]}{\partial x_j} = 0\\
&\frac{\partial(\overline{\rho}\widetilde{e}_0)}{\partial t} + \frac{\partial[\overline{\rho}\widetilde{u}_j\widetilde{e}_0 + \widetilde{u}_j\overline{p} + \overline{u_j'' p} + \overline{\rho u_j'' e_0''} + \overline{q}_j - \overline{u_i\tau_{ij}}]}{\partial x_j}\\
&= 0
\end{aligned} \tag{10}$$

In these equations, $\widetilde{e}_0$ is the density averaged total energy:

$$\widetilde{e}_0 = \widetilde{e}_0 + \frac{\widetilde{u}_k\widetilde{u}_k}{2} + \frac{\widetilde{u_k'' u_k''}}{2} \tag{11}$$

It is usual to rewrite unknown terms as:

$$\begin{aligned}
&\overline{\tau_{ji}} = \widetilde{\tau_{ji}} + \overline{\tau_{ji}''}\\
&\overline{u_j'' p} + \overline{\rho u_j'' e_0''} = C_p\overline{\rho u_j'' T} + u_i\overline{\rho u_i'' u_j''} + \frac{\overline{\rho u_j'' u_i'' u_i''}}{2}
\end{aligned} \tag{12}$$

$$\begin{aligned}
&\overline{q_j} = -\overline{C_p\frac{\mu}{Pr}\frac{\partial T}{\partial x_j}} = -C_p\frac{\mu}{Pr}\frac{\partial\widetilde{T}}{\partial x_j} - C_p\frac{\mu}{Pr}\frac{\partial\overline{T''}}{\partial x_j}\\
&\overline{u_i\tau_{ij}} = \widetilde{u}_i\widetilde{\tau}_{ij} + \overline{u_i''\tau_{ij}} + \widetilde{u}_i\overline{\tau_{ij}''}
\end{aligned} \tag{13}$$

where $Pr$ is the Prandtl number. Moreover, we have neglected the molecular viscosity ($\mu$) fluctuations.

Favre-averaged Navier-Stokes equations present different properties than Reynolds-averaged Navier-Stokes. For example, there is no mass flux across the Favre-averaged streamlines [105, 106]. However, in homogeneous flows (those whose statistics of turbulent fluctuations are independent of position [107]) it can be shown that Favre averaging and ensemble average give identical results. A discussion of advantages and drawbacks of Favre-averaging is found in [106].

Incompressible, non-heat conducting flows are described completely by the velocity field. In this case the divergence-free condition couples the pressure with the velocity. In compressible flows the pressure is determined by an equation of state.

In compressible flows we can split the turbulent fluctuations in a compressible and an incompressible parts. The incompressible part of this splitting can be understood as the part of the solution that satisfies the incompressible Navier-Stokes equations, and the compressible part is the remainder. However, there is no general decomposition based on this approach useful for the analysis, since there is no explicit distinction between acoustic waves and other compressible events [90].[1] Kovasznay [108] introduced linearized theory based on a small parameter expansion to obtain a decomposition of compressible turbulent fluctuations. Thus, these fluctuations can be considered as combinations of acoustical, vortical and entropy modes. Although the validity of this assumption is restricted, this decomposition is useful since it gives considerable insight of this kind of flows. Following this approach, it is possible intermodal energy transfer in addition to interscale energy transfer. Hence the increasing complexity in modeling compressible turbulence.

The number of terms of (10) to be modeled is bigger than in the incompressible case. Unfortunately, it has been shown that the models based on the extension of those developed originally for incompressible flows fail to adequately predict turbulent flows at high Mach numbers, and a specific work is required for compressible flows.

An important concept is that of *isotropy*. In case of turbulent flows, isotropy usually means direction invariance. Experiments seems to confirm the hypothesis of local isotropy is reasonable for the flow smaller scales. However most turbulence models are developed under the assumption of isotropy in all the range of scales, which possibly introduce errors in the solution.

Second-order closure models [109–111] abandon the Boussinesq hypothesis. These methods introduce a differential equation for each component of the Reynolds stresses, and another equation to determine the dissipation. This approximation removes the isotropy assumption of the Boussinesq hypothesis, and it accounts for phenomena such as flows over curved surfaces. However, the numerical resolution of these models presents problems due to instability. Moreover, several terms of the exact transport equations for the components of the Reynolds stresses are unknown and the modeling of these terms introduces again the Boussinesq hypothesis.

We refer the interested reader to [92] for a thorough discussion of these methods.

Even though it is fair to acknowledge the importance of RANS methods in the development of turbulence computations, there is a theoretical issue that is important to remember. When we average the Navier–Stokes equations, the nature of the equations change. A deterministic phenomenon is expressed in terms of a set of statistic equations. If we accept that the Navier–Stokes equations describe correctly the dynamics of a flow, there is a contradiction with the statistical approach of averaging. In this context the approach of Large Eddy Simulation allows to circumvent this contradiction.

[1] When the nonlinear mechanism of the flow is dominant it is possible to use the Helmholtz decomposition of the compressible velocity field, but without a direct decomposition of the other variables [90].

### 2.4 Large Eddy Simulation

Large Eddy Simulation (LES) of turbulent flows is a different strategy to solve turbulent flow problems. Turbulent flows are characterized by vortices with a wide range of length and time scales. Biggest vortices have a size comparable to the length size of the mean flow. On the other hand, the dissipation of kinetic energy occurs at the smaller scales. The idea of LES is to model only the scales that are not solved by the numerical scheme. Ideally, the smallest size of the resolved scales is determined by the grid size, and then the *subgrid scales* (SGS) are those of a size smaller than the grid size. However, the numerical method may introduce dispersion and dissipation errors even in scales captured by the grid. Thus, in current LES models SGS terms include scales bigger than the grid size but not well resolved by the numerical method. The separation of this scales is performed by means of *filtering*. Thus, *subfilter* scales (SFS) instead of SGS models is a more suitable term. We consider a resolved scale as a scale whose wavenumber is below the cut-off frequency of the numerical method.

The filtering operation has to fulfill some requirements [89]

1. Constant preservation

$$\overline{a} = a, \quad a \in \mathbb{R} \tag{14}$$

2. Linearity,

$$\overline{\Phi + \Psi} = \overline{\Phi} + \overline{\Psi}, \tag{15}$$

3. Commutation with derivation:

$$\frac{\overline{\partial \Phi}}{\partial s} = \frac{\partial \overline{\Phi}}{\partial s}, \quad \text{with } s = \boldsymbol{x}, t \tag{16}$$

Many filters have been used in literature, among them we can cite the volume-average box filter [112] and the Gaussian filter [113]. In the context of structured grids, LES with Padé filters [2, 4, 5] has obtained very good results. However, filtering for unstructured grid is more difficult. In particular, the development of commutative filters for this kind of grids is specially complex. The use of MLS has been proposed [114], and also other approaches based on Least-Squares [115], or in discrete triangular filters with weights assigned to each vertex [116].

Most turbulence models are developed under the assumption of Boussinesq hypothesis, and therefore, they suppose

isotropic flows. This assumption does not hold for a vast majority of flows in nature. However, in LES formulations the idea is to apply the turbulence model only to the smaller scales. In this context, the assumption of isotropy in these scales is more reasonable. Another advantage of the LES approach is that the Navier-Stokes equations are not averaged, keeping their deterministic nature.

### 2.4.1 The Filtered Navier-Stokes Equations

In the following, super index $\bar{}$ indicates filtered variables. Favre-filtered variables ($\tilde{\Phi} = \overline{\rho\Phi}/\overline{\rho}$) are denoted with $\tilde{}$. Quantities denoted by $\hat{}$ are computed according its definition but from filtered variables. Prime $'$ variables are used for the small scale part of the variables. We define the small scale as the subfilter part of a variable, $u_i' = u - \tilde{u}$.

Following [117, 118], the filtered compressible Navier Stokes equations, for the conservative variables ($\overline{\rho}, \overline{\rho}\tilde{u}, \overline{\rho}\tilde{v}, \overline{\rho}\tilde{w}, \overline{\rho}\hat{E}$) are

$$\begin{aligned}
&\frac{\partial \overline{\rho}}{\partial t} + \frac{\partial (\overline{\rho}\tilde{u}_j)}{\partial x_j} = 0 \\
&\frac{\partial (\overline{\rho}\tilde{u}_i)}{\partial t} + \frac{\partial (\overline{\rho}\tilde{u}_i\tilde{u}_j + \overline{p}\delta_{ij} - \hat{\tau}_{ij})}{\partial x_j} = -\frac{\partial (\overline{\rho}\sigma_{ij})}{\partial x_j} + \beta_i \\
&\frac{\partial \overline{\rho}\hat{E}}{\partial t} + \frac{\partial [(\overline{\rho}\hat{E} + \overline{p})\tilde{u}_j - \hat{\tau}_{ij}\tilde{u}_i + \hat{q}_j]}{\partial x_j} \\
&\quad = -\alpha_1 - \alpha_2 - \alpha_3 + \alpha_4 + \alpha_5 - \alpha_6
\end{aligned} \tag{17}$$

The term $\overline{\rho}\sigma_{ij} = \overline{\rho}(\widetilde{u_i u_j} - \tilde{u}_i\tilde{u}_j)$ represents the subgrid stresses and $\beta_i$ is:

$$\beta_i = \frac{\partial (\overline{\tau}_{ij} - \hat{\tau}_{ij})}{\partial x_j} \tag{18}$$

$\beta_i$ arises from the nonlinearity of the viscous stress. We define the total resolved energy $\hat{E} = \overline{p}/(\gamma - 1) + \frac{1}{2}\overline{\rho u_i \rho u_j}/\overline{\rho}$, and $\overline{p}$ is the filtered pressure. Subgrid terms in the energy equation are:

$$\begin{aligned}
\alpha_1 &= \tilde{u}_i \frac{\partial \overline{\rho}\sigma_{ij}}{\partial x_j}, & \alpha_2 &= \frac{1}{\gamma - 1}\frac{\partial (\overline{pu}_j - \overline{p}\tilde{u}_j)}{\partial x_j} \\
\alpha_3 &= \overline{p\frac{\partial u_j}{\partial x_j}} - \overline{p}\frac{\partial \tilde{u}_j}{\partial x_j}, & \alpha_4 &= \overline{\tau_{ij}\frac{\partial u_i}{\partial x_j}} - \overline{\tau_{ij}}\frac{\partial \tilde{u}_j}{\partial x_j}
\end{aligned} \tag{19}$$

$$\alpha_5 = \frac{\partial (\tilde{u}_i\overline{\tau}_{ij} - \tilde{u}_i\hat{\tau}_{ij})}{\partial x_j}, \qquad \alpha_6 = \frac{\partial (\overline{q}_j - \hat{q}_j)}{\partial x_j} \tag{20}$$

$\alpha_1$ is the SGS dissipation and $\alpha_2$ is the pressure-velocity subgrid term, which describes the effect of subgrid turbulence on the conduction of heat in the resolved scales. The term $\alpha_3$ is the pressure-dilatation correlation. On the other hand, $\alpha_4$ is related to the SGS molecular dissipation. Moreover $\alpha_5$ is the SGS diffusion due to molecular transport of momentum, and $\alpha_6$ is the SGS diffusion due to molecular transport of heat. This is not the only possible formulation. Thus, it is possible to modify the thermodynamic variables to obtain other expressions of the compressible LES filtered equations [90, 119].

Subgrid stresses, $\overline{\rho}\sigma_{ij}$, are usually expressed as the sum of three terms:

$$\overline{\rho}\sigma_{ij} = \overline{\rho}(\widetilde{\tilde{u}_i\tilde{u}_j} - \tilde{u}_i\tilde{u}_j) + \overline{\rho}(\widetilde{u_i'\tilde{u}_j} + \widetilde{\tilde{u}_i u_j'}) + \overline{\rho}(\widetilde{u_i' u_j'}) \tag{21}$$

The first term is the Leonard stress tensor, which represents a relation between filtered quantities. The second is the cross-term stress. It accounts for the interactions between resolved and unresolved scales. The third term represents the SGS Reynolds stresses, which relates only subgrid quantities.

Classical LES models for compressible flow start from these equations and introduce a SGS model, for example the Smagorinsky [120] or the more advanced Dynamic Smagorinsky [121, 122] models. Terms $\alpha_3$–$\alpha_6$ and $\beta_i$ are neglected under the assumption that they are smaller than the SGS modeled terms [123]. One of the main assumptions in the modeling of SGS terms for compressible flow is the incompressibility of the subgrid scales, that is, compressibility only affects the large scales.

### 2.4.2 Current Techniques

One of the main drawbacks of classical LES techniques is that the SGS model is in fact applied to the whole range of scales. Current LES techniques try to modify only the range of scales that are unresolved. From a physical standpoint, these methods try to take into account the interaction between the unresolved scales and the smallest resolved scale. Interactions between largest scales of the flow and subgrid scales are neglected.

The *Variational Multiscale Method* (VMS) [124–127] is a different approach to Large Eddy Simulation. It uses variational projections instead of filtered-equations. This fact avoids the problems caused by non-commutative filters. In their formulation, they decompose the solution space of the Navier-Stokes equation into large and small scales. Later, the VMS framework was extended to a three-level approach where the scales are divided in coarse, fine and unresolved scales [128]. In earlier versions of VMS, the idea is to apply the subscale model to the unresolved scales, whereas large and small scales are solved directly. A more recent approach [129] is the Residual-based subgrid-scale modeling. In this approach, the problem of solving the Navier-Stokes equations is divided in two problems: obtaining approximate solutions to the fine-scale problem (that involves the unresolved scales) and the resolution of the coarse-scale problem (that involves the coarse and fine scales). The solution

of the fine-scale problem is inserted in the coarse-scale problem. Interactions between coarse and fine scales are included in the formulation without addition of any eddy-viscosity model. In practice, the fine-scale problem is not solved exactly. Instead an approximate expression is used [129].

The VMS method could be included in a class of methods of *Multi-level Simulations* [89]. These methods try to solve an equation for the subgrid terms, and it seems that currently they are the preferred for the research community. Among these Multi-level techniques, we can cite methods with several grid levels [130, 131] or methods that use several filtering levels [132].

Another method is the *Approximated Deconvolution Model* (ADM) [133]. The idea of this method is to recover the unfiltered solution with an approximated deconvolution and the application of a relaxation term to model the effect of subgrid scales on the resolved scales.

Usual SGS models for LES are computed from filtered variables. In [117, 134] a *High Pass Filtered* (HPF) model is used. The idea of this method is to use high-pass filtered variables instead of filtered variables to compute the SGS model terms. In [118] it is shown an analogy between the VMS and filtering in LES. In this framework, the HPF model may also be related to the VMS method.

A successful technique in structured grids is the use of high-resolution compact finite differences with the addition of an explicit filter [2, 4, 5]. These techniques are usually called "no model" methods. However, there is an implicit SGS model in them: the filter. Padé filters depend on a parameter. Depending on this parameter, the amount of filtering changes, according to its transfer function. In practice, the amount of filtering is selected following stability criteria. Since the filtering has only (ideally) a dissipative action, backscatter is not modeled. This approach is also related with the ADM method, since the ADM process is equivalent to filtering a wider range of high frequencies [135].

The spirit of this approach is similar to that of *Implicit Large-Eddy Simulation* (ILES) techniques. The main assumption in ILES is that the action of the subgrid scales on the resolved scales is purely dissipative. In these methods, the numerical discretization introduces the amount of dissipation needed without explicit subgrid modeling. In LES the energy cascade process is truncated since the smaller scales are not solved by the grid. However, there are methods used in LES that introduce certain amount of dissipation. Thus, it is legitimate to ask if it is convenient the use of a dissipative SGS model with these methods. The use of upwind methods for LES is controversial [136, 137], due to the excessive dissipation in coarse grids. On the other hand, in [138] it is shown that the amount of dissipation of upwind discretizations mainly depends on the quality of the approximation of the derivatives. The use of upwind methods for LES has been proposed in [139–144] without using any SGS model. This approach is the *Monotonically Integrated Large-Eddy Simulation* (MILES). In some of the MILES approaches, the physical viscosity is set to zero [145], and all the viscosity (molecular also) is introduced by the numerical method. However, this approach presents consistency problems. The main drawback of the MILES approach is the lack of physical foundation. Even though from a numerical point of view the method obtains goods results, there is no solid physical basis for this approach. However, there are some theoretical advances [144], that relate the form of certain terms of the discretized equations with a subgrid tensor. Since the numerical method also plays the role of a dissipation model, it is very important the numerical scheme used in these techniques. Not all the methods are valid for use in MILES, since they have to mimic the dissipation of energy at the smaller scales [146].

## 3 Computational Aeroacoustics

The sound generation by a flow and its propagation are a matter of aerodynamics. Indeed, the conservation equations of mass and momentum govern both the flow dynamics and the resulting acoustic phenomena. However, the features of the aerodynamic flow and the sound are different. The first is convective and/or diffusive and the second is propagative with very low attenuation due to viscosity. On the other hand, aeroacoustic problems present a wider range of wavelengths than those of aerodynamic ones.

Aeroacoustic noise optimization is the main topic of many widespread research studies of industrial interest [147–149]. In fact, the noise level emitted by a device could determine the success or failure of a new prototype. On the other hand turbomachines are widely found in industrial applications. In these devices the level of sound generated is a very important parameter of design.

The prediction of aerodynamic noise benefits from recent developments in numerical methods and computer science. However, despite the knowledge accumulated over the past few decades on the mechanisms of noise generation on complex systems as for example air delivery systems, the prediction of such a flow field and the resulting acoustic pressure, by numerical methods is still difficult. This is due to our inability to model the turbulent viscous flow with enough accuracy on complex geometries and to the complicated nature of flow through turbomachines. Until now, there is still no consensus about the aeroacoustic approach to adopt, and actually, it depends on the application. In the following we present a succinct description of the most commonly used approaches.

Previously to our exposition, we recall the concepts of far and near-fields. The concept of far-field, relative to the effects of the flow compressibility, concerns the propagation of acoustic waves produced by a pressure change in the

propagation medium. The occurred disturbance propagates gradually by molecular excitement to the observer located far from the source. Unlike the far-field, near-field includes the sound due to the fluid compressibility and another component called the aerodynamic disturbance field or pseudo-sound. It consists of all pressure fluctuations governed primarily by the incompressibility directly related to the flow. These fluctuations are local and are not propagative.

In Computational Aeroacoustics (CAA), two computational approaches are possible:

*Direct Approach* This approach consists of adjusting the aerodynamic numerical modeling to the acoustics requirements. In other words, it is needed to use numerical schemes adapted to the acoustic propagation, providing low-dissipation and low-dispersion. However, the complexity of implementing these schemes and the far field constraint, where the grid must extend over very large distances, greatly increases the computational costs and makes using this approach very difficult for complex geometries.

*Hybrid Approach* This approach can be divided into two types of modeling.

- The first one is to use the direct approach near disturbances in which the acoustic waves are propagated over a short distance. They are then propagated using an adapted propagation operator, as Kirchhoff's equation [150] for example, to the far field. For adapted wave operator we mean a wave equation or other conservation equation system that permits an acoustic wave to propagate from a given acoustic source. However, the simulation of the flow field requires DNS or LES, and the treatment of boundary conditions must be done with utmost care to ensure an accurate transition between near and far fields.
- The second consists of separating aerodynamics and acoustics computations. This is possible when the Mach number of the flow is small [151]. Thus, acoustic sources are given by aerodynamic calculation and propagated using wave equation (Ffowcs Williams-Hawkings [153], Kirchhoff, ...), linearized Euler equations (LEE) or other approaches like linearized perturbed compressible equations (LPCE) [154], ... The constraints and the computation time is considerably reduced compared to DNS.

### 3.1 Aeroacoustics of Complex Geometries

Aeroacoustics is a science dealing with the sound generated either by the flow itself, as free jet turbulence or by its interaction with a moving or static surface, rigid or deformable, as fan blades, helicopter rotor, compressors or turbines, etc. Thus, in these latter kinds of applications, we need to deal with flow through complex geometries.

The first attempt to formulate a theory about the acoustics of propellers was conducted by Lynam and Webb [155] in 1919. They showed that the rotation of the blades of a propeller causes a periodic modulation of the fluid flow and associated acoustic disturbance. Another approach, initiated by Bryan [156] in 1920, is to study the propagation of a source point in uniform motion. This had as main feature the introduction of the concept of delayed time.

Gutin [157] was the first to establish a theoretical formalism of a steady noise source through linear acoustics. He showed that steady aerodynamic forces correspond to dipole source distribution on the disc of a propeller. This model proves to be incomplete because, in reality, the noise emitted by rotating blades extends rather high frequencies. The sound at high frequencies is a consequence of the unsteadiness of aerodynamic loads.

Advances in the prediction of noise from the airflow, are based on of Lighthill's [158, 159] investigations. In his analogy, the generated noise is mathematically reduced to the study of wave propagation in a medium at rest, in which the effect of the flow is replaced by a distribution of sources. The pressure is therefore regarded as characterizing a sound field of small amplitude carried by a fluid, whose properties are uniform throughout the area at rest. The major intake of Lighthill is to include nonlinear terms expressing the noise generation by turbulent flow.

Curle [160] extended the Lighthill's analogy to include solid boundaries by treating them as distributions of surface loads. Subsequently, Ffowcs Williams and Hawkings (FW&H) [153] have extended this approach by taking into account the motion of solid surfaces in the flow.

*Limits of Aeroacoustic Analogy and Alternative Approaches* In the common formulation of aeroacoustic analogy solution, the noise is radiated in free and far field. As strong hypotheses: reflections, diffractions, scattering as well as the confinement effects are not taken into account. These hypotheses make very easy the use aeroacoustic analogy for noise prediction of open rotors or free jets for example, but they are also its weaknesses in case of confining. In [149] it was shown that using the FW&H formulation to model the noise generated by a centrifugal fan does not match measurements because of the presence of a casing. Taking into account the sound attenuation of the casing to correct the directivity has not really solved the problem. For this kind of problems, it was therefore concluded that the aeroacoustic analogy does not obtain accurate results.

To take into account confining effects, it is expected that LEE can give satisfactory results. In fact, with LEE one can use the same acoustic sources as FW&H for example, and in addition reflections, diffractions and scattering are naturally taken into account by an adequate choice of boundary conditions.

*Linearized Euler Equations* In many aeroacoustic applications we can assume that problems are linear [151]. In those cases, it is possible to linearize the Euler equations around a (mean) stationary solution $\boldsymbol{U}_0 = (\rho_0, u_0, v_0, p_0)$. Thus, we can write the Linearized Euler Equations written in conservative form are the following:

$$\frac{\partial \boldsymbol{U}}{\partial t} + \frac{\partial \boldsymbol{F}}{\partial x} + \frac{\partial \boldsymbol{G}}{\partial y} + \boldsymbol{H} = \boldsymbol{S} \tag{22}$$

In (22) $\boldsymbol{S}$ a source term and

$$\boldsymbol{U} = \begin{pmatrix} \rho \\ \rho u \\ \rho v \\ p \end{pmatrix} \qquad \boldsymbol{F} = \begin{pmatrix} \rho u_0 + \rho_0 u \\ p + \rho_0 u_0 u \\ \rho_0 u_0 v \\ u_0 p + \gamma p_0 u \end{pmatrix} \tag{23}$$

$$\boldsymbol{G} = \begin{pmatrix} \rho v_0 + \rho_0 u \\ \rho_0 v_0 u \\ p + \rho_0 v_0 v \\ v_0 p + \gamma p_0 v \end{pmatrix}$$

$$\boldsymbol{H} = \begin{pmatrix} 0 \\ (\rho_0 u + u_0 \rho)\frac{\partial u_0}{\partial x} + (\rho_0 v + v_0 \rho)\frac{\partial u_0}{\partial y} \\ (\rho_0 u + u_0 \rho)\frac{\partial v_0}{\partial x} + (\rho_0 v + v_0 \rho)\frac{\partial v_0}{\partial y} \\ (\gamma - 1) p \nabla \cdot \boldsymbol{v_0} - (\gamma - 1)\boldsymbol{v} \cdot \nabla p_0 \end{pmatrix} \tag{24}$$

where $\boldsymbol{v} = (u, v)$ is the perturbation in velocity, $\boldsymbol{v_0} = (u_0, v_0)$, $\rho$ is the perturbation in density, $p$ is the perturbation in pressure and $\gamma = 1.4$. In case of an uniform mean flow, $\boldsymbol{H}$ is null. To solve these equations, we need to compute previously the acoustic sources $\boldsymbol{S}$, by using LES or DNS. In [152] is presented a methodology to compute the sources.

## 4 The FV-MLS Method

The Finite Volume method is one of the most usual numerical techniques for the resolution of fluid dynamics problems in complex geometries on unstructured grids [1, 17, 161]. The main problem for achieving higher-order accuracy when these methods are used with unstructured grids is the computation of the gradients and successive derivatives required for the reconstruction of the variables inside the cells by Taylor approximations. Moreover, the accuracy in the computations of the gradients is also important in the computation of viscous fluxes in the case of the Navier-Stokes equations. The first attempts to obtain finite volume methods with order higher than one were the Monotone Upstream Schemes for Conservation Laws (MUSCL) [13]. One drawback of this technique is the lack of multidimensionality, since it is based on the direct extension of the one-dimensional approach.

One technique that has achieved the least dissipative results for hyperbolic problems is the so called *Residual Distribution* or *Fluctuation Splitting* techniques [61–79]. The main problem of this technique is that it is based on a conservative linearization of the inviscid flux, which is not always available. Moreover the viscous flux discretization and the extension to orders of accuracy higher than two are not straightforward. Other authors compute the gradients by using the Least-Squares technique or reconstructions based on the Green-Gauss theorem [16, 19, 22, 162]. However, by using these techniques it is no easy to find convergence orders higher than two. The *k-exact* reconstruction [18, 163, 164] is based on the computation of a polynomial expansion inside each cells that preserves the mean of the variable in that cell. This polynomial expansion reconstructs exactly polynomials up to order $k$. The coefficients defining this polynomial are chosen by minimization, in the Least-Squares sense, of the difference between the averages of the reconstructing polynomial and the actual averages. Moreover, geometric weights are included to measure the relative importance of the error incurred at each control volume. These weights are functions of the distance. These constraints in the Least-Squares problems makes mandatory the resolution of the Least-Squares problem each time step. This technique has problems with boundary-layer grids and in the computation of viscous fluxes. Recently, a generalization of the *k-exact* reconstruction is introduced in [165, 166]. More information about high-order methods for unstructured grids can be found in [86].

The basic idea of the FV-MLS method [80, 81, 85, 167] is to use Moving-Least Squares [82–84] approximations to compute the derivatives required for the finite volume scheme. The MLS method, and in general Reproducing Kernel methods [83, 84], have been widely used in surface reconstruction and by the meshless community. It is able to obtain accurate approximations of a variable and its derivatives from a scattered set of data. Thus, it is very convenient for use with unstructured grids in a finite volume framework. Moreover, the centered nature of the MLS approximations makes it very suitable for the computation of viscous terms. Thus, viscous fluxes are directly computed at integration points whereas for convective terms an upwind discretization is used.

The usual approach of high-order finite volume schemes is pragmatic and *bottom-up*. Starting from an underlying piecewise constant representation, a discontinuous reconstruction of the field variables is performed at the cell level. An important practical consequence is that the discretization of higher order terms requires some kind of *recovery* procedure, which is, almost invariably, inconsistent with the aforementioned reconstruction. Our approach is somewhat the opposite. We start from a high-order and highly regular representation of the solution, obtained by means of

Moving Least-Squares approximations [82]. This approach is directly suitable for the discretization of elliptic/parabolic equations and high-order spatial terms. For equations with a predominantly hyperbolic character, the global representation is *broken* locally, at the cell level, into a piecewise polynomial reconstruction, which allows to use the finite volume technology of Godunov-type schemes for hyperbolic problems (e.g. Riemann solvers, limiters).

### 4.1 General Formulation

Consider a system of conservation laws of the form

$$\frac{\partial \boldsymbol{u}}{\partial t} + \nabla \cdot (\boldsymbol{\mathcal{F}}^H + \boldsymbol{\mathcal{F}}^E) = \boldsymbol{S} \quad \text{in } \Omega \tag{25}$$

supplemented with suitable initial and boundary conditions. The fluxes have been generically split into a hyperbolic-like part, $\boldsymbol{\mathcal{F}}^H$, and an elliptic-like part, $\boldsymbol{\mathcal{F}}^E$. Consider, in addition, a partition of the domain $\Omega$ into a set of non-overlapping *control volumes* or *cells*, $\mathcal{T}^h = I$. Furthermore, we define a reference point (*node*), $\boldsymbol{x}_I$ inside each cell (the cell centroid).

The spatial representation of the solution is as follows: consider a function $\boldsymbol{u}(\boldsymbol{x})$, given by its point values, $\boldsymbol{u}_I = \boldsymbol{u}(\boldsymbol{x}_I)$, at the cell centroids, with coordinates $\boldsymbol{x}_I$. The approximate function $\boldsymbol{u}^h(\boldsymbol{x})$ belongs to the subspace spanned by a set of *basis functions* $\{N_I(\boldsymbol{x})\}$ associated to the nodes, such that $\boldsymbol{u}^h(\boldsymbol{x})$ is given by

$$\boldsymbol{u}^h(\boldsymbol{x}) = \sum_{j=1}^{n_{\boldsymbol{x}}} N_j(\boldsymbol{x}) \boldsymbol{u}_j \tag{26}$$

which states that the approximation at a point $\boldsymbol{x}$ is computed using certain $n_{\boldsymbol{x}}$ surrounding nodes. This set of nodes is referred to as the *stencil* associated to the evaluation point $\boldsymbol{x}$. In particular, the above approximation is constructed using Moving Least-Squares (MLS) approximation [82]. Note that, using MLS, the approximate function $\boldsymbol{u}^h(\boldsymbol{x})$ is not a polynomial in general. The *centered* character of the approximation avoids the spatial bias which is often found in patch-based piecewise polynomial interpolation. MLS shape functions values at a point depend on the number of neighbors considered for this point ($n_{\boldsymbol{x}}$), a kernel function and a basis [167]. In this work we use a polynomial basis and the following exponential kernel, defined in 1D as:

$$W(x, x^*, s_x) = \frac{e^{-(\frac{d}{c})^2} - e^{-(\frac{dm}{c})^2}}{1 - e^{-(\frac{dm}{c})^2}} \tag{27}$$

with $d = |x_j - x^*|$, $d_m = 2\max(|x_j - x^*|)$, with $j = 1, \ldots, n_{x^*}$, $c = \frac{d_m}{s_x}$, $x^*$ is the position of a reference point, $x$ is the position of every cell centroid of the stencil and $s_x$ is a shape parameter. A 2D kernel is obtained by multiplying two 1D kernels. Thus, the 2D exponential kernel is the following:

$$W_j(\boldsymbol{x}, \boldsymbol{x}^*, s_x, s_y) = W_j(x, x^*, s_x) W_j(y, y^*, s_y) \tag{28}$$

The integral form of the system of conservation laws (25) for each control volume $I$ is:

$$\int_{\Omega_I} \frac{\partial \boldsymbol{u}}{\partial t} \, d\Omega + \int_{\Gamma_I} (\boldsymbol{\mathcal{F}}^H + \boldsymbol{\mathcal{F}}^E) \cdot \boldsymbol{n} \, d\Gamma = \int_{\Omega_I} \boldsymbol{S} \, d\Omega \tag{29}$$

Introducing the component-wise reconstructed function $\boldsymbol{u}^h$ we obtain

$$\int_{\Omega_I} \frac{\partial \boldsymbol{u}^h}{\partial t} \, d\Omega + \int_{\Gamma_I} (\boldsymbol{\mathcal{F}}^{hH} + \boldsymbol{\mathcal{F}}^{hE}) \cdot \boldsymbol{n} \, d\Gamma = \int_{\Omega_I} \boldsymbol{S}(\boldsymbol{u}^h) \, d\Omega \tag{30}$$

For hyperbolic problems, we introduce a "*broken*" reconstruction, $\boldsymbol{u}_I^{hb}$, which approximates $\boldsymbol{u}^h(\boldsymbol{x})$ (and, therefore, $\boldsymbol{u}(\boldsymbol{x})$) locally inside each cell $I$, and is discontinuous across cell interfaces [81, 86]. In general, we require the order of accuracy of the broken reconstruction to be the same as that of the original continuous reconstruction. Thus, using Taylor series expansions; a quadratic reconstruction inside cell $I$, reads

$$\boldsymbol{u}_I^{hb}(\boldsymbol{x}) = \boldsymbol{u}_I^h + \nabla \boldsymbol{u}_I^h \cdot (\boldsymbol{x} - \boldsymbol{x}_I) + \frac{1}{2} (\boldsymbol{x} - \boldsymbol{x}_I)^T \boldsymbol{H}^h (\boldsymbol{x} - \boldsymbol{x}_I) \tag{31}$$

where the gradient $\nabla \boldsymbol{u}_I^h$ and the Hessian matrix $\boldsymbol{H}^h$ involve the successive derivatives of the continuous reconstruction $\boldsymbol{u}^h(\boldsymbol{x})$, which are evaluated at the cell centroids using MLS. This dual continuous/discontinuous reconstruction of the solution is crucial in order to obtain accurate and efficient numerical schemes for mixed parabolic/hyperbolic problems. The cell-wise broken reconstruction defined here is actually a piecewise continuous approximation to $\boldsymbol{u}^h$. The advantage is that it allows to make use of Riemann solvers, limiters, and other standard finite volume technologies, while keeping some consistency in terms of functional representation. Thus, the general continuous reconstruction is used to evaluate the viscous (elliptic-like) fluxes, whereas its discontinuous approximation is used to evaluate the inviscid (hyperbolic-like) fluxes.

The final semidiscrete scheme for the continuous/discontinuous approach can be written as

$$\int_{\Omega_I} \frac{\partial \boldsymbol{u}^h}{\partial t} \, d\Omega + \int_{\Gamma_I} \boldsymbol{H}(\boldsymbol{u}^{hb+}, \boldsymbol{u}^{hb-}) \, d\Gamma + \int_{\Gamma_I} \boldsymbol{\mathcal{F}}^{hE} \cdot \boldsymbol{n} \, d\Gamma = \int_{\Omega_I} \boldsymbol{S}(\boldsymbol{u}^h) \, d\Omega \tag{32}$$

where $\boldsymbol{H}(\boldsymbol{u}^{hb+}, \boldsymbol{u}^{hb-})$ is a suitable numerical flux.

Time integration scheme requires special attention. It has been shown [168] that at most third order of accuracy is achieved by using an explicit time integration scheme with a *zero-mean* reconstruction [18, 169]. This problem is avoided by using mass lumping formulations or implicit time integration techniques [168].

### 4.2 1D Linear Advection Equation Analysis

In the following, we expose the analysis of the discretization of the 1D linear advection equation with the third-order FV-MLS method. This analysis will allow us to evaluate the behavior of the FV-MLS method in the approximation of convective terms of a transport equation. We note that this analysis is only valid for equally-spaced nodes, but it will be useful to compare with other existing methods and to get a flavor of the behavior of the numerical scheme. In this analysis we analyze the spatial discretization only, without taking into account the effects of time integration. For a study of the effects of third and fourth order Runge-Kutta explicit schemes we refer the reader to [167].

The 1D linear advection equation reads

$$\frac{\partial u}{\partial t} + a\frac{\partial u}{\partial x} = 0 \tag{33}$$

on the domain $0 \leq x \leq 2\pi$, with an harmonic wave as initial condition:

$$u(x,0) = g(0)e^{ikx} \tag{34}$$

and that also verifies that $u(0) = u(2\pi)$. In (33), $u$ is a scalar quantity propagating with phase velocity $a$. In order to make the exposition easier to follow, we consider only $a > 0$. However, the conclusions will be valid for any value of $a$.

With this initial setup, the solution of the problem is written as:

$$u(x,t) = g(t)e^{i\kappa x} \tag{35}$$

Thus, introducing (35) in (33):

$$\frac{dg}{dt}e^{i\kappa x} + ia\kappa g e^{i\kappa x} = 0 \tag{36}$$

that is,

$$\frac{dg}{dt} = -ia\kappa g \tag{37}$$

and consequently $g(t)$ is

$$g(t) = g(0)e^{-ia\kappa t} \tag{38}$$

where $g(0)$ is the initial value of $g(t)$. Thus, we have:

$$u(x,t) = g(0)e^{i(\kappa x - a\kappa t)} \tag{39}$$

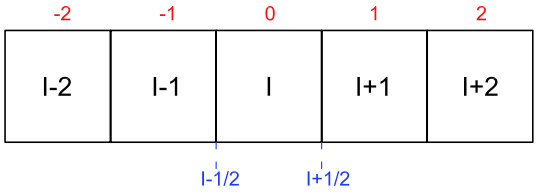


**Fig. 1** 1D Spatial discretization scheme

On the other hand, an initial wave can be obtained by the addition of initial conditions of the form (34):

$$u(x,0) = \sum_{q=1}^{F} g_q(0)e^{i\kappa_q x} \tag{40}$$

where $F$ is the number of Fourier modes.

Due to the linearity of (33), the solution can be obtained by the addition of solutions of the form (39). Thus, for $F$ modes we obtain:

$$u(x,t) = \sum_{q=1}^{F} g_q(0)e^{i\kappa_q(x-at)} \tag{41}$$

A real wavenumber $\kappa$ is related to a real frequency $\omega = a\kappa$, such that (41) is a solution of (33). The relationship between frequency and wavenumber is called *dispersion relation*. For (33) this relationship is linear, that is a characteristic feature of wave propagation in non-dispersive media. Thus, the velocity of propagation is the same for all the wavenumbers.

The discretization of (33) usually introduces a dispersion error. This means that in the numerical solution of (33), waves with different wavenumber propagate with different velocities. Moreover, if the modified wavenumber is complex, dissipation errors will appear.

The linearity of the solution allows us to perform the analysis for a single Fourier mode (see (40)), so the subindex $q$ is omitted.

In contrast with a finite difference discretization, where we use point values of the variable, a finite volume scheme refers to the mean value of the variables inside a control volume $I$.

$$\tilde{u}_I = \frac{1}{\Delta x}\int_{x_L}^{x_R} u\,dx \tag{42}$$

where $x_R$ and $x_L$ are the values of the $x$-coordinate of the cell $I$ interfaces $I + \frac{1}{2}$ and $I - \frac{1}{2}$, as is plotted in Fig. 1.

The FV-MLS method uses the integral form of (33):

$$\frac{\partial}{\partial t}\int_{x_L}^{x_R} u\,dx = -(f(x_R,t) - f(x_L,t)) \tag{43}$$

where $f(u) = au$ is the flux function. by using the mean value definition (42) of $u(x)$, the spatial discretization of

(43) reads as:

$$\frac{\partial \tilde{u}_I}{\partial t} = -\frac{a}{\Delta x}(u^*_{(I+\frac{1}{2})} - u^*_{(I-\frac{1}{2})}) \tag{44}$$

In (44), $u^*$ refers to the reconstruction of the value of $u$ at integration points ($I \pm \frac{1}{2}$). After some algebra, we obtain the modified wavenumber of the third order FV-MLS scheme. The interested reader is referred to [167] for the complete process. Note that this is a time-dependent problem, and in this analysis we have introduced the correction terms required for the conservation of the mean (*zero-mean*) of the third-order scheme [81, 168].

Here, we only point out that the modified wavenumber of the third order FV-MLS scheme is:

$$\kappa^* = \frac{Z^*}{i} \tag{45}$$

with

$$\begin{aligned} Z^* = 1 - e^{-i\kappa\Delta x} &+ \sum_{l=-P}^{Q} \frac{\partial N_{(I+l)}}{\partial x}(e^{i\kappa l\Delta x} - e^{i\kappa(l-1)\Delta x})\left(\frac{\Delta x}{2}\right) \\ &+ \frac{1}{2}\sum_{l=-P}^{Q} \frac{\partial^2 N_{(I+l)}}{\partial x^2}(\widetilde{A}e^{i\kappa l\Delta x} - \widetilde{B}e^{i\kappa(l-1)\Delta x}) \end{aligned} \tag{46}$$

and

$$\widetilde{A} = \left(\frac{\Delta x}{2}\right)^2 - \frac{1}{\Delta x}\int_I (x - x_I)^2\, dx \tag{47}$$

$$\widetilde{B} = \left(\frac{\Delta x}{2}\right)^2 - \frac{1}{\Delta x}\int_{(I-1)} (x - x_{(I-1)})^2\, dx \tag{48}$$

Note that $\widetilde{A}$ and $\widetilde{B}$ include the zero-mean terms. If we only consider the spatial discretization error, we can write [167]

$$\frac{a^*}{a} = \frac{Z^*}{i\kappa\Delta x} \tag{49}$$

The modified phase velocity $a^*$ is the numerical propagation velocity of a harmonic function. When $a^*$ and $a$ are different, dispersion errors appear in the numerical solution. As the original equation (33) is non-dispersive, the numerical solution of an harmonic function with different wavenumbers loses the original shape.

The real part of the modified wavenumber is related to dispersion errors, whereas the imaginary part is related to dissipation errors. Upwinding introduces a non-null imaginary part in the modified wavenumber of the FV-MLS method. Although this could be seen as a drawback in terms of accuracy, we note the remarkable property that most of the dissipation is introduced in the wavenumbers that are not accurately resolved for the numerical method. This fact can indeed be seen as an implicit low-pass filtering of the spurious waves.

*Remark 1* This is an interesting feature of the numerical scheme, since it is going to be used on unstructured grids. On this kind of grids, the anisotropy of the elements may originate additional spurious waves. The implicit filtering helps to attenuate the distortion of the solution by these waves.

In Fig. 2 we plot the real and the imaginary parts of the scaled modified wavenumber versus the real scaled wavenumber for different values of the kernel shape parameter $s_x$. Resulting curves show the dispersion and dissipation errors of the third-order FV-MLS numerical scheme. We observe the strong dependence of the properties of the numerical method with the choice of the kernel parameter. Moreover, its properties also depend on the kind of kernel [167].

For a problem with non-harmonic waves, the crests of the waves propagate with the phase speed but the energy of the wave packet propagate with the group velocity $v_g = a\frac{\partial \kappa^*}{\partial \kappa}$ (see [170]). The phase speed and the group velocity of the third-order FV-MLS method are shown in Fig. 3.

In Fig. 4 we plot a comparison between the third and second-order FV-MLS method and the first order upwind scheme in terms of dispersion and dissipation error. It is clear the improvement in the properties of the numerical scheme by increasing the order.

*Remark 2* Note that the main source of differences between two different finite volume methods, in terms of dispersion and dissipation properties, is the accuracy on the computation of the derivatives, provided the numerical flux functions are the same. Thus, it is very important an accurate computation of the derivatives. In multidimensional problems and in a finite volume framework, it is also important a multidimensional character of the computation of the derivatives.

#### 4.2.1 A Numerical Benchmark for Simulation of Wave Propagation

In this section we solve the first problem presented in the *First ICASE/LaRC Workshop on Benchmark Problems in Computational Aeroacoustics* [171]. We solve (33) in the domain $-20 \leq x \leq 450$ with the following initial condition:

$$u(x, 0) = 0.5e^{[-\ln(2)(\frac{x}{3})^2]} \tag{50}$$

The transported wave may be considered as the addition of a number of harmonic waves with different frequencies and amplitudes. If the numerical scheme is not able to simulate accurately the propagation of waves with very different frequencies the numerical solution will be a very distorted wave.

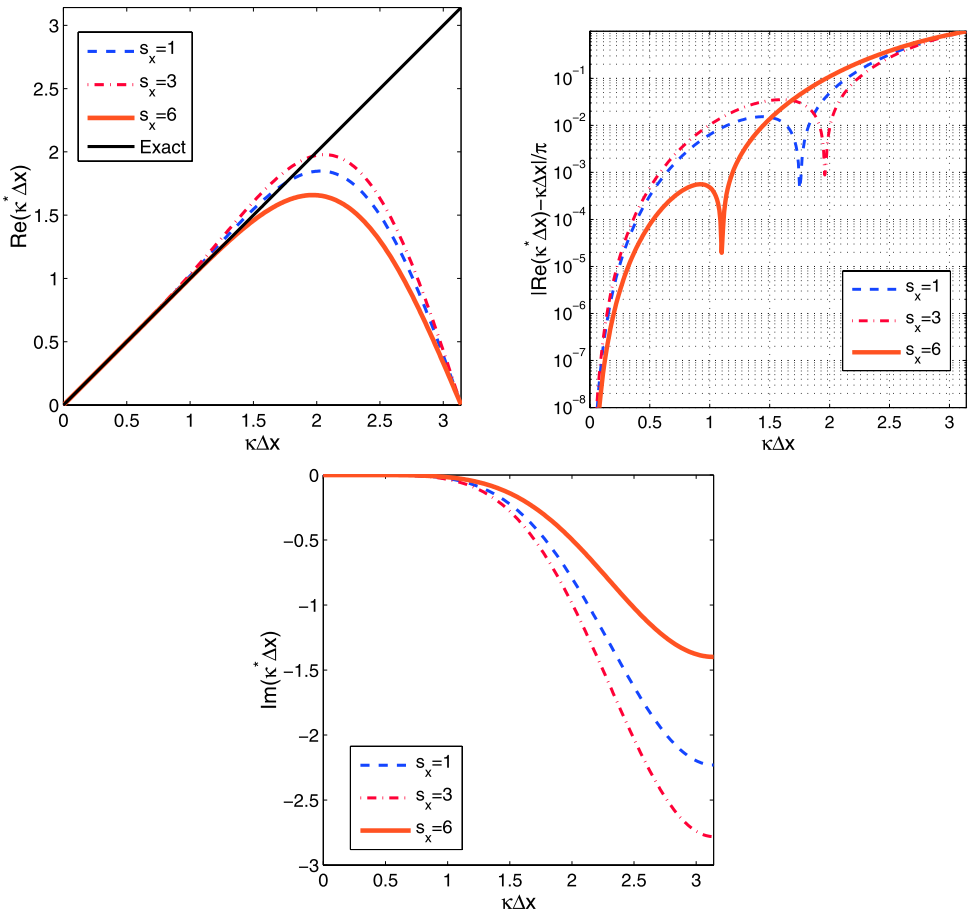


**Fig. 2** Dispersion and dissipation curves of the third-order FV-MLS method for different values of the kernel shape parameter $s_x$. *On the top*, we plot the real part of the modified scaled wavenumber, related to the dispersion of the numerical scheme (*left*) and the dispersion error in logarithmic scale (*right*). *On the bottom*, we plot the imaginary part of the modified scaled wavenumber, related to dissipation

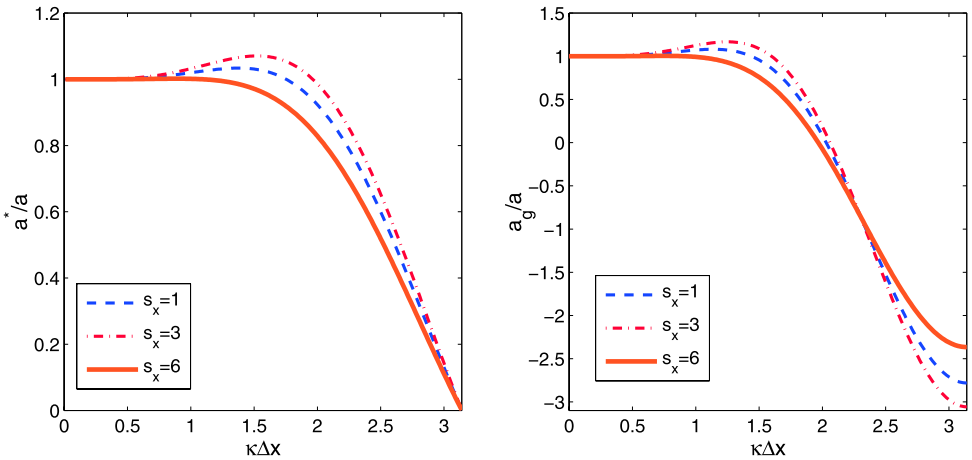


**Fig. 3** Phase-speed (*left*) and group velocity (*right*) of the third-order FV-MLS method for different values of the kernel shape parameter $s_x$

In Fig. 5 we show the results for the second order FV-MLS method. We observe that the solution is not accurate, as it presents a very distorted wave. The results with the second-order FV-MLS scheme are equivalent to the results of the MUSCL scheme using centered fourth-order differences (this result only holds for 1D [167]).

In order to improve the resolution, we increase the order of the numerical scheme. In figure 6 we plot the results for the third-order FV-MLS method at non-dimensional times $t = 100$, $t = 400$. For this grid spacing ($\Delta x = 1$) the solution is somewhat dissipative, and the wave shape presents a certain amount of distortion for $t = 400$. However, the dispersion and dissipation errors of the wave are smaller than those of other higher-order methods as the fourth-order MacCormack method presented in [172], or fourth-order centered finite differences [173].

From the present analysis, it is clear the importance of a good resolution of a given numerical scheme for the res-

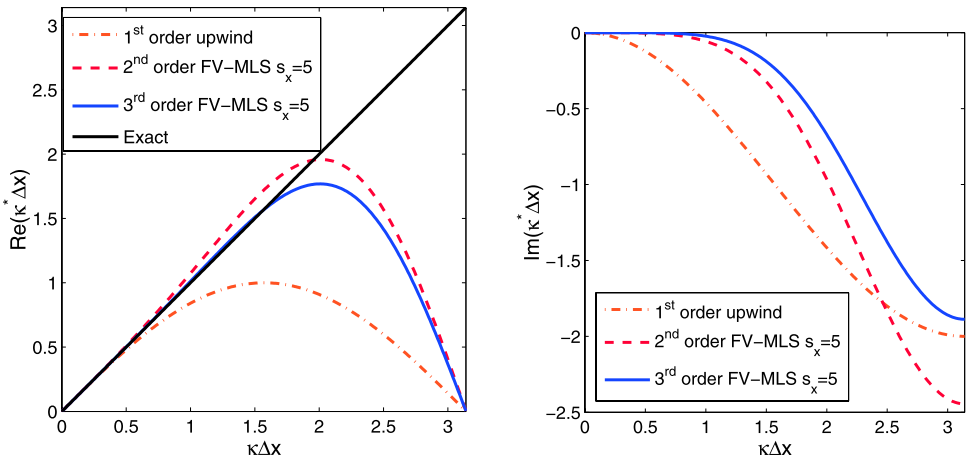


**Fig. 4** Influence of the order of the approximation for the FV-MLS method. *On the left*: Real part of $\kappa^* \Delta x$ versus $\kappa \Delta x$. *On the right*: Imaginary part of $\kappa^* \Delta x$ versus a $\kappa \Delta x$

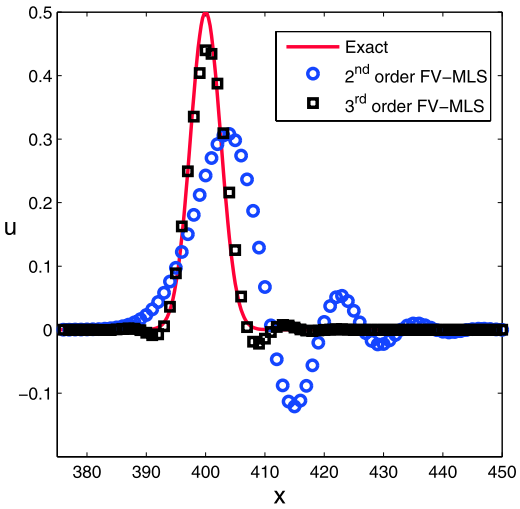


**Fig. 5** Second and third-order FV-MLS solution for the first problem presented in [171] at a non-dimensional time $t = 400$, with $CFL = 0.6$, exponential kernel $s_x = 6$, $\Delta x = 1$

olution of wave propagating problems. Thus, not only the dissipative errors are important but also phase errors, which may lead to a inaccurate solution. It is important that a numerical scheme solves accurately the widest possible range of frequencies. Even though on unstructured grids the main procedure to improve the resolution is increasing the order of the numerical scheme, it is important to note that two different numerical methods with the same order of accuracy may have very different dispersion and dissipation curves. Thus, the use of a higher-order method does not imply a more accurate solution.

## 5 Implicit Filtering for Turbulence Computations

We have just seen that the kernel function determines the properties of the FV-MLS scheme. It is possible to see dissipation and dispersion curves in terms of resolved scales. Thus, in Fig. 2, we see that the numerical scheme introduces dispersion and dissipation errors for a given frequency (cut-off frequency). We recall that we consider a resolved scale as a scale whose wavenumber is below the cut-off frequency of the numerical method. From the dissipation curve we observe that frequencies over the cut-off frequency are naturally dissipated by the numerical method. This dissipation has to mimic the high-wavenumber end of the inertial subrange. The spirit of this approach follows closely the MILES method.

The methodology presented in [5] for the computation of turbulent flows uses a no-model approach. The numerical method is based on quasi-spectral compact finite differences and the addition of an explicit Padé filter. The explicit filter removes the energy of the highest frequencies, and the amount of energy removed is controlled by the parameter of the Padé filter. Here, we follow a similar procedure, but the filter is implicitly defined in the numerical model. Thus, the shape parameter of the exponential kernel $s$ acts as the filter parameter. The dissipation curve in Fig. 2 gives a flavor of the shape of the implicit filter.

On the other hand, in compressible flow simulations it is possible the presence of shocks in the solution. An usual approach with finite volume methods is the use of slope-limiters [19, 20]. However, the use of slope-limiters presents some drawbacks. One of the main drawbacks of slope limiters is the limiting in smooth regions. In these regions, limiting is not needed, and the introduction of additional numerical dissipation reduces the accuracy of the numerical scheme. One possible solution is the selective-limiting approach, in which a shock detector decides if the slope-limiter is applied or not. There are many shock-detectors developed in the literature. Among others, we can cite [21, 174–178]. Here, the additional dissipation introduced by the slope-limiter is restricted by the MLS-based shock detector developed in [86, 87]. It allows to keep the high-order of the numerical scheme except in the vicinity of shocks (where

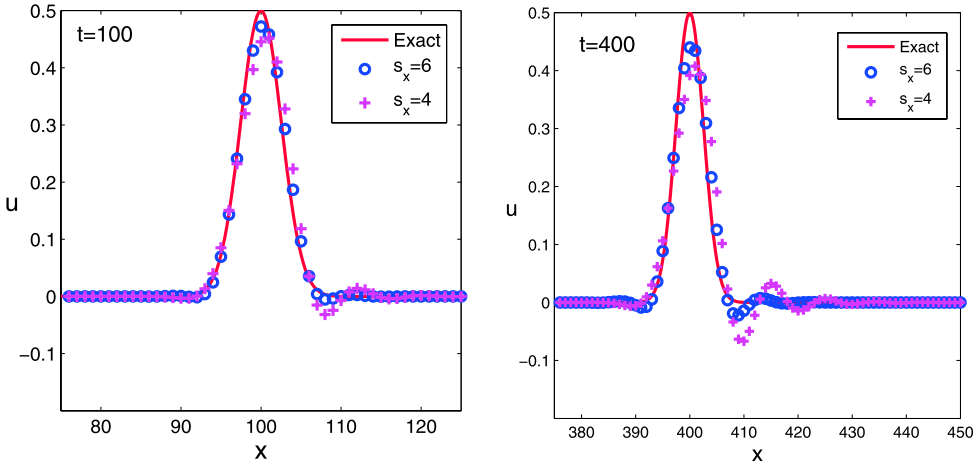


**Fig. 6** Third-order FV-MLS solution for the first problem presented in [171] at different non-dimensional times, with $CFL = 0.6$, $\Delta x = 1$, exponential kernel and several values of the shape parameter $s_x$

it is first-order accurate). Thus, in our approach the limiting method is only used to prevent oscillations near shocks, not to mimic the small-scale dissipation. This is a remarkable difference with other implicit LES approaches based on non-oscillatory finite volume schemes [142–144]. In fact, the dissipation for the SGS model is controlled by the $s$ parameter of the kernel.

### 5.1 Decay of Compressible Isotropic Turbulence

In this section we present the application of the third-order FV-MLS method to the computation of a turbulent flow. We solve the decay of compressible isotropic turbulence. Even though this example is the simplest case of turbulent flow, it is very interesting since it allows to check if the numerical method is able to mimic the dissipation of the subfilter scales. The numerical model has to predict the evolution of a turbulent region without walls or any mechanism to remove or add energy, nor to organize the larger eddies.

The computational domain is $[0, 2\pi]^3$. We have imposed periodic boundary conditions in all directions [138]. The setup of the problem is the same as case 6 in [179]. The turbulence length scale is defined by selecting the initial three-dimensional energy spectrum as

$$E_{3D} \propto k^4 \exp\left[-2\left(\frac{k}{k_p}\right)^2\right] \tag{51}$$

where $k_p = 4$ is the wavenumber corresponding to the peak of the spectrum and $k$ is the wavenumber. Following [180], we define $\chi$, as the ratio of compressible kinetic energy to the total turbulent kinetic energy. In this example, $\chi = (\frac{q^d}{q})^2 = 0.2$, where $q$ is the root mean square magnitude of the fluctuation velocity, and $q^d$ is the root mean square magnitude of the dilatational fluctuation velocity. We note that $\chi$ is an indicator of the level of compressibility of the flow. $\chi = 0$ corresponds to an incompressible flow.

The initial velocity fluctuations are specified to obtain a turbulent Mach number, $M_t = \frac{q}{c} = 0.4$, where $c$ is the mean speed of sound. In this simulation, the initial values are given by:

$$\begin{aligned} (\rho'_{rms})^2/\langle\rho\rangle^2 &= 0.032 \\ (T'_{rms})^2/\langle T\rangle^2 &= 0.005 \end{aligned} \tag{52}$$

We recall that symbol $\langle\ \rangle$ refers to mean value and primes denote fluctuating variables.

The third-order FV-MLS scheme has been used for the computations, with the MLS-based sensor [87] and the Barth and Jespersen limiter [19]. We have tested two levels of refinement. The coarse grid with $32^3$ elements and the finest grid with $64^3$ elements. An explicit fourth-order Runge-Kutta scheme has been used for time integration. The time step is $\Delta t = 0.05$, corresponding approximately to 250 time-steps per eddy turnover time ($\tau_0$) (the eddy turnover time is defined as the ratio of the turbulent kinetic energy to the dissipation rate based on the initial field).

Our "reference solution" is a LES calculation on a $128^3$ grid, computed with sixth-order compact finite differences and a explicit Padé filter with parameter $\alpha = 0.49$ [5]. The result of this LES coincides with the DNS solution of [179].

In Figs. 7 and 8 we plot the results obtained on the $32^3$ and $64^3$ grids, for different values of the kernel shape parameter $s_x$ for the time evolution of the turbulent kinetic energy, $K = \langle\rho[(u')^2 + (v')^2 + (w')^2]\rangle$, and the energy spectrum. Results agree very well with those of the reference solution. The choice of $s_x$ has an influence on the results. Thus, the value of $s_x = 5$ is somewhat under dissipative. The origin of this under dissipation is probably related with an excess of energy in the range of the resolved scales for this value of the parameter, as it is shown in Fig. 8. We note the two different slopes appearing in the results of the three-dimensional energy spectrum. This result agrees with the Eddy-Damped Quasi-Normal Markovian Theory (EDQNM), which predicts that the slope of the inertial range of the irrotational

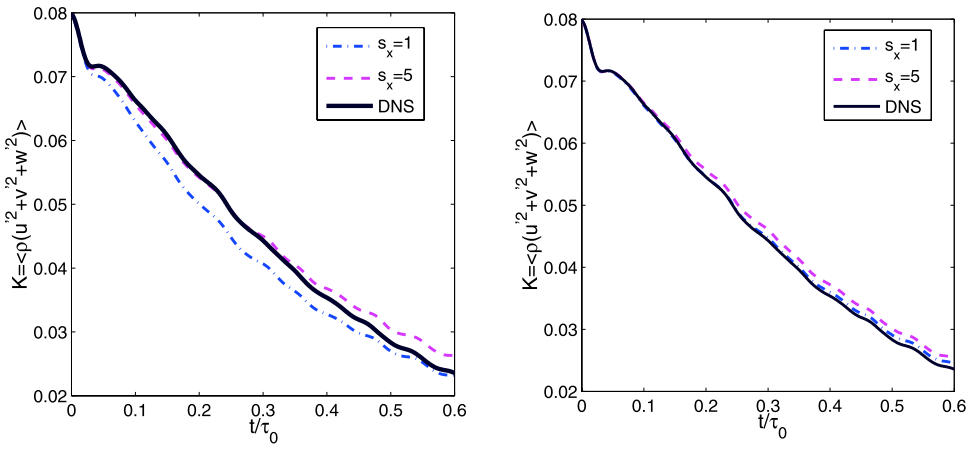


**Fig. 7** Effect of the shape parameter $s_x$ on time history of turbulent kinetic energy decay. Results for the $32^3$ mesh (*left*) and for the $64^3$ mesh (*right*)

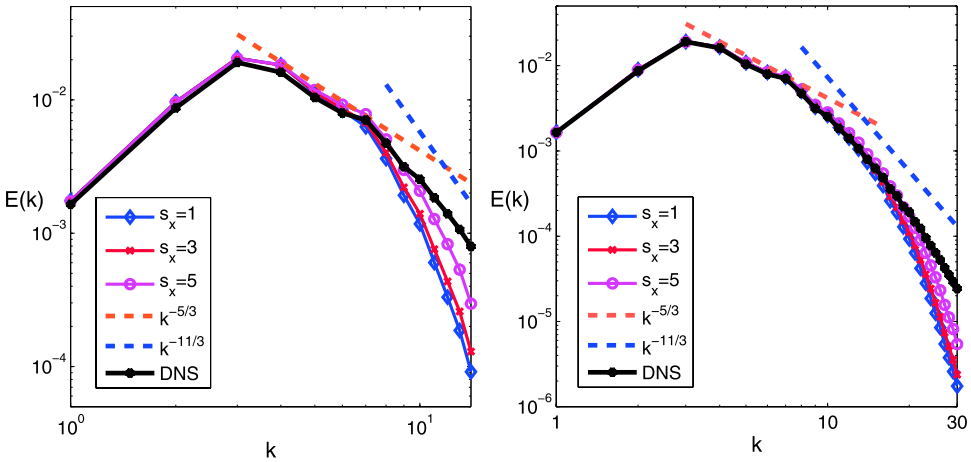


**Fig. 8** Instantaneous three-dimensional energy spectra at $t/\tau_0 = 0.3$. Effect of the shape parameter $s_x$. Results for the $32^3$ mesh (*left*) and for the $64^3$ mesh (*right*)

velocity correlation depends on time [181, 182]. On a convective time scale, it is proportional to $k^{-5/3}$, whereas in a viscous time scale it is proportional to $k^{-11/3}$.

In order to compare the accuracy of this approach we show in Fig. 9 the results of this approach and the results of a fourth-order centered finite difference method. We note that these results are also more accurate than the results obtained with an standard third-order finite volume scheme [5]. The origin of this greater accuracy relies on the high quality of the computations of derivatives with MLS. Moreover, we believe that the excessive dissipation usually attributed to upwind methods is not consequence of the upwinding process but of the poor quality of the derivatives computed [138].

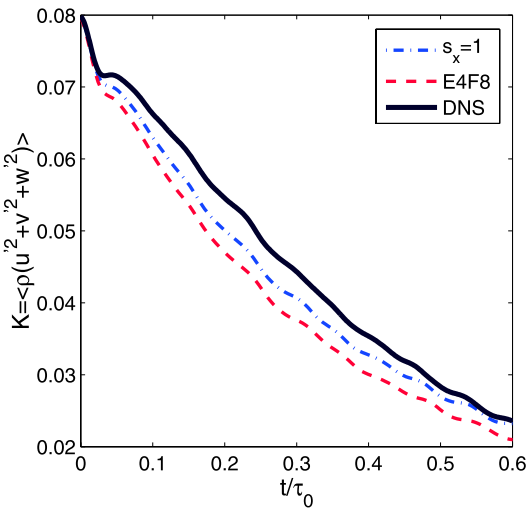


**Fig. 9** Time history of turbulent kinetic energy decay. Comparison between third-order FV-MLS results and a centered fourth-order finite differences method with an eighth-order filter [5]. Results for the $32^3$ mesh

## 6 Selected Aeroacoustics Examples

In this section we present the results of the application of the FV-MLS method to the resolution of some selected aeroacoustic problems on unstructured grids, by using the Linearized Euler Equations.

In CAA the treatment of boundary conditions plays a key role [183], since even small spurious disturbances when

the waves leave the domain can distort the acoustic field. In the following we expose our approach to the boundary conditions. For our modeling, the boundary conditions enter in the discretized equations through a proper definition of the numerical flux that can be written as $\boldsymbol{H}(\boldsymbol{U}^+, \boldsymbol{U}^{*-})$ (see (32)), where $\boldsymbol{U}^{*-}$ is the external state variable. Depending on the boundary type, the construction of $\boldsymbol{U}^{*-}$ accounts for, both, the physical boundary conditions that must be enforced and the information leaving the domain.

*Reflecting Boundary Conditions* A perfectly reflecting boundary condition is easily obtained by defining, at each Gauss points on the rigid wall boundaries, an external mirror fictitious state $\boldsymbol{U}^{*-}$.

The external state is then expressed as

$$\boldsymbol{U}^{*-} = \boldsymbol{R}\boldsymbol{U}^{+} \tag{53}$$

where $\boldsymbol{R}$ is a transition matrix function of $\boldsymbol{n}$'s components, it reads

$$\boldsymbol{R} = \begin{pmatrix} 1 & 0 & 0 & 0 \\ 0 & 1-2n_x^2 & -2n_x n_y & 0 \\ 0 & -2n_x n_y & 1-2n_y^2 & 0 \\ 0 & 0 & 0 & 1 \end{pmatrix} \tag{54}$$

Using this condition, the mass flux computed by the Riemann solver is zero and the non-permeability condition is satisfied.

*Absorbing Boundary Conditions* Constructing absorbing (non-reflecting) boundary conditions for CAA is pretty delicate because of the high sensitivity of the accuracy to the small spurious wave reflexions at far field boundaries. Approaches based on the characteristics theory are not suited for CAA problems, other approaches, such as Perfectly Matched Layers (PML) [184] and radial boundary condition [185] are more indicated and widely discussed in the literature for finite differences schemes.

In this work we employ upwinding technique used by Bernacki et al. [186] with DG to select only outgoing waves at the outer boundaries. Intuitively, it means that the wave is completely dissipated at boundaries, but unfortunately nothing proves that energy is actually dissipated and no spurious wave reflexions persist. To overcome this problem, we join to the above procedure a grid stretching zone [187]. Grid stretching transfers the energy of the wave into increasingly higher wavenumber modes and the numerical scheme removes this high-frequency content. This is the same idea as the one exposed for the implicit SGS modeling. With this process most of the energy of the wave is dissipated before reaching the boundaries.

At the grid stretching zone, it is possible to use the MLS method as a filter in unstructured grids. The filtering process is developed by the application of a MLS reconstruction of the variables, i.e.:

$$\bar{\boldsymbol{U}}(\boldsymbol{x}) = \sum_{j=1}^{n_{x_I}} \boldsymbol{U}(\boldsymbol{x}) N_j(\boldsymbol{x}) \tag{55}$$

where, $\boldsymbol{U}$ is the reconstructed variable, $\bar{\boldsymbol{U}}$ is the filtered variable and $N$ is the MLS shape function. This reconstruction is performed by using a kernel with shape parameters favoring dissipative behavior as those used to the approximation of the variables. The value of these parameters determines the range of frequencies to be filtered.

At the outer boundaries, we propose the following explicit numerical flux,

$$\boldsymbol{H}(\boldsymbol{U}^n, \boldsymbol{U}^{*n}, \boldsymbol{n}) = \frac{1}{2}(\mathbb{F}(\boldsymbol{U}^n)\cdot\boldsymbol{n} + |\mathbb{P}|\boldsymbol{U}^{n-1}) \tag{56}$$

with, $\boldsymbol{U}^{*n}$ is the fictitious state corresponding to the absorbing side ensuring $\mathbb{P}\boldsymbol{U}^{*n} = |\mathbb{P}|\boldsymbol{U}^{n-1}$. $\mathbb{P}$ is the Jacobian matrix of system (22) and $|\mathbb{P}| = \mathbb{V}^{-1}|\mathbb{D}|\mathbb{V}$. $\mathbb{D}$ and $\mathbb{V}$ are respectively, eigenvalues diagonal matrix and eigenvectors matrix of $\mathbb{P}$. $|\mathbb{P}|$ then is given by

$$|\mathbb{P}| = \begin{pmatrix} L_3 & \frac{n_x}{2c_0}(-L_1+L_2) & \frac{n_y}{2c_0}(-L_1+L_2) & \frac{-1}{c_0^2}L_3 + \frac{1}{2c_0}(L_1+L_2) \\ 0 & \frac{n_x^2}{2}(L_1+L_2)+n_y^2 L_4 & \frac{n_x n_y}{2}(L_1+L_2-2L_4) & \frac{n_x}{2c_0}(-L_1+L_2) \\ 0 & \frac{n_x n_y}{2}(L_1+L_2-2L_4) & \frac{n_y^2}{2}(L_1+L_2)+n_x^2 L_4 & \frac{n_y}{2c_0}(-L_1+L_2) \\ 0 & \frac{n_x c_0}{2}(-L_1+L_2) & \frac{n_y c_0}{2}(-L_1+L_2) & \frac{1}{2}(L_1+L_2) \end{pmatrix} \tag{57}$$

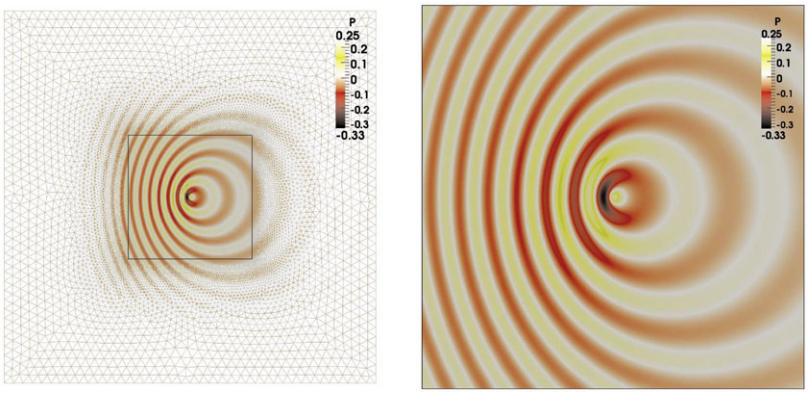


**Fig. 10** Radiation of a monopolar source in a subsonic ($M = 0.5$) uniform mean flow. $200 \times 200$ unstructured grid and acoustic pressure at $t = 270$

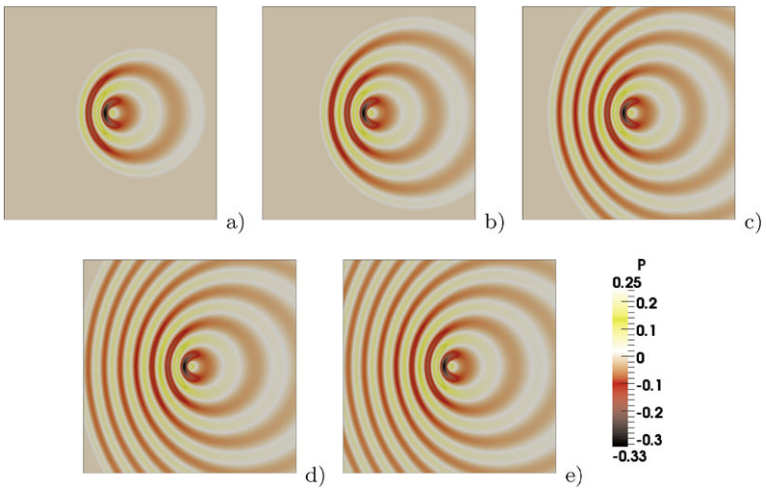


**Fig. 11** Radiation of a monopolar source in a subsonic ($M = 0.5$) uniform mean flow. Acoustic pressure at different times (a) $t = 60$, (b) $t = 90$, (c) $t = 150$, (d) $t = 210$, (e) $t = 270$

where,

$$\begin{aligned} L_1 &= |\boldsymbol{V_0} \cdot \boldsymbol{n} - c_0| \\ L_2 &= |\boldsymbol{V_0} \cdot \boldsymbol{n} + c_0| \\ L_3 &= L_4 = |\boldsymbol{V_0} \cdot \boldsymbol{n}| \end{aligned} \tag{58}$$

with, $\boldsymbol{V_0} = (u_0, v_0)$ and $c_0$ the speed of sound.

### 6.1 Convected Monopole

This case reproduces the example of [188]. The radiation of a monopole source is computed in a subsonic mean flow, with Mach number $M_x = 0.5$. The source is located at $x_s = y_s = 0$, and is defined as:

$$\boldsymbol{S}_p = \frac{1}{2} \exp\left( -\ln(2) \frac{(x - x_s)^2 + (y - y_s)^2}{2} \right) \sin(\omega t) \times [1, 0, 0, 1]^T \tag{59}$$

where the angular frequency is $\omega = 2\pi/30$ and $t$ is the time coordinate. The wave length is $\lambda = 30$ units, and the computational domain is a square with 200 units for each side. The source term is made dimensionless with $[\rho_0 c_0/\Delta x, 0, 0, \rho_0 c_0^3/\Delta x]^T$. This a very good test case to check the ability of the FV-MLS to simulate the propagation of acoustic waves on an unstructured grid. With the aim of testing the stability and the behavior of the proposed method for the boundary conditions, an unstructured grid absorbing layer has been added. The absorbing layer is placed from the boundary of the computational domain to $x = \pm 300$ and $y = \pm 300$. In Fig. 10 it is shown the unstructured grid used for the resolution of this problem. To build this grid, 800 equally spaced nodes at the circumference of the computational domain are used and 120 nodes at the outer boundaries circumference.

In addition to the absorbing boundary condition given by (56), the shape filter parameters of the absorbing layer are $s_x = s_y = 8$ [187].

A fifth-order mass matrix-based FV-MLS solver is used for this example [168].

Two acoustic waves propagate upstream and downstream of the source, and due to the effect of the mean flow, the apparent wavelength is modified and it is different upstream ($\lambda_1 = (1 - M_x)\lambda$) and downstream ($\lambda_2 = (1 + M_x)\lambda$) of the source.

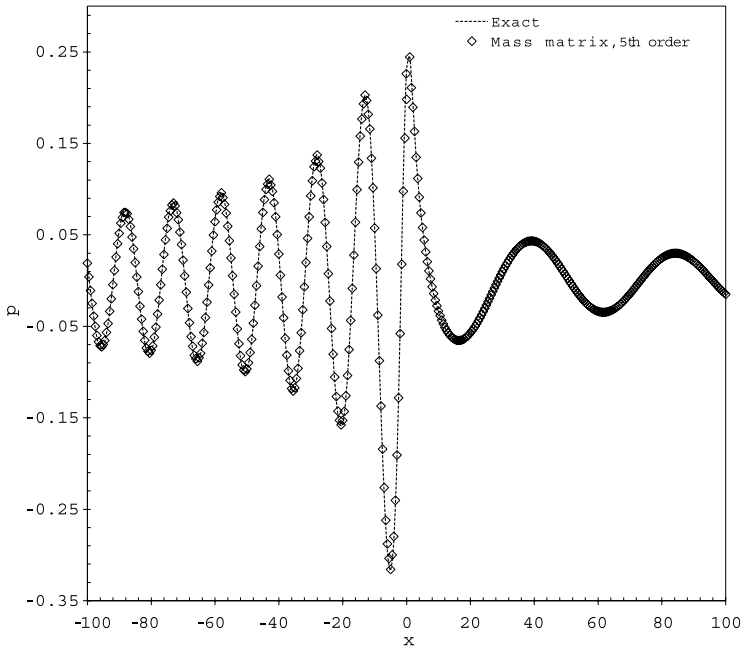


**Fig. 12** Radiation of a monopolar source in a subsonic ($M = 0.5$) uniform mean flow. Acoustic pressure profile along axis $y = 0$ at $t = 270$

In Fig. 11 pressure isocontours for different non-dimensional times $t$ are shown. The pressure profile along axis $y = 0$ at time $t = 270$ is reproduced in Fig. 12, and also matches the results in [188].

In order to check the stability of the boundary conditions, we let the computations to continue until 180 periods of the source. This time is enough for the wave to reach outer boundaries. Comparing the pressure field with the one corresponding to $t = 270$ (9 source periods), it is observed that there is no change in the solution. The acoustic wave is completely dissipated by the buffer zone when it lefts the computational domain, see Fig. 10.

## 6.2 Acoustic Waves Propagation into a Centrifugal Fan

The centrifugal fan noise is usually dominated by tones produced by the impeller blade passage. The resultant tonal noise corresponds to the blade passage frequency and its higher harmonics. This is a consequence of the strong interaction between the impeller and the diffuser blades at their interface.

Shrouded impellers are usually used in high-rotational speed centrifugal fans. The impellers are linked downstream by a vaned diffuser, see Fig. 13.

A methodology based on a hybrid modeling of the aeroacoustic behavior of a high-rotational speed centrifugal fan is presented in this section. The main objective of this example is to visualize the wave propagation into a centrifugal turbomachine and demonstrate, then, the power of the proposed methodology. Linearized Euler's equations are used to propagate noise radiated by the rotor/stator interaction. The fluctuating forces at the interaction zone are obtained

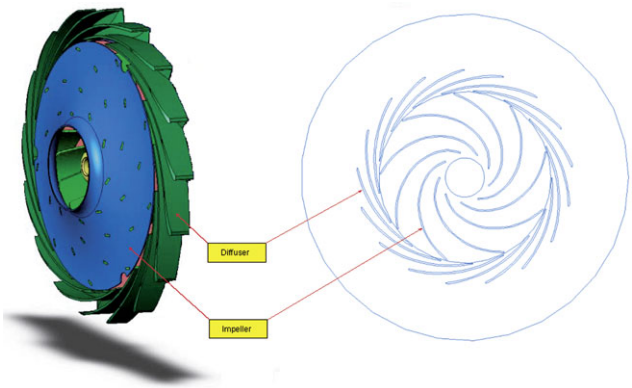


**Fig. 13** 3D and 2D centrifugal fan geometry

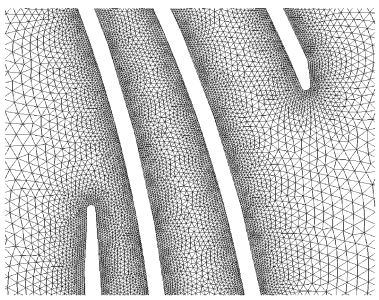

**Fig. 14** Detail of the unstructured grid at the diffuser blades

by an aerodynamic study of the centrifugal fan presented in [149, 189]. In this section we calculate the acoustic wave propagation of a centrifugal fan with a 9-bladed rotor and a diffuser with 17 blades, as shown in Fig. 13. For the computations we use an unstructured grid, with at least 10 points

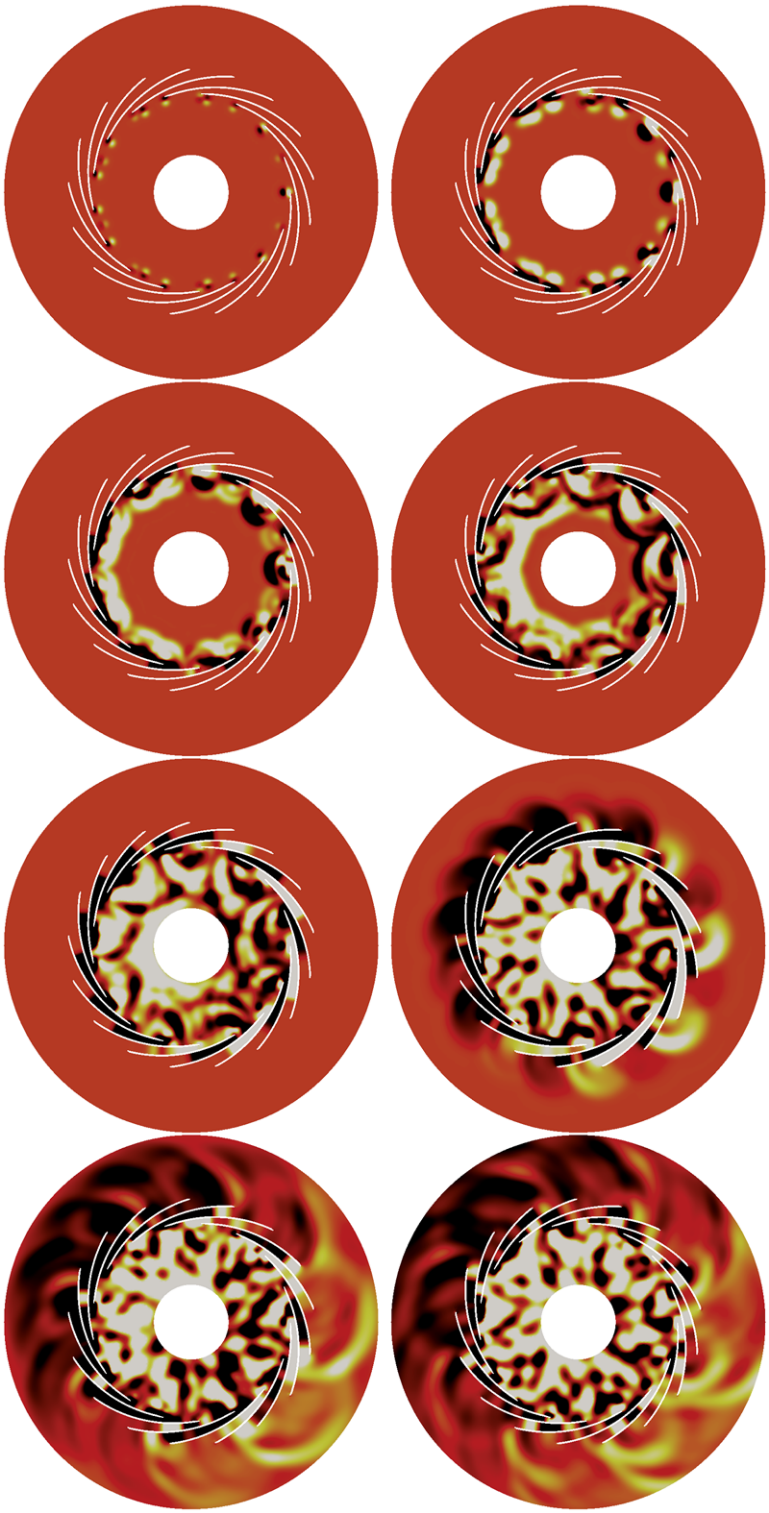

**Fig. 15** Acoustic pressure history for the acoustic waves propagation into a centrifugal fan

per wavelength. A detail of the unstructured grid used in this problem is shown in Fig. 14.

*Sources Modeling* If we refer to FW&H analogy [153], one can identify three acoustic sources of three different natures:

- Monopole or thickness source: it is a surface distribution due to the volume displacement of fluid during the motion of surfaces.
- Dipole source or loading source: it is a surface distribution due to the interaction of the flow with the moving bodies.

– Quadrupole source: it is a volume distribution due to the flow outside the surfaces.

When the quadrupole source is included, substantially more computational resources are needed for volume integration. However, in many subsonic applications the contribution of the quadrupole source is small. Thus, we have neglected it in this calculation. Moreover, the monopolar source is also neglected at low Mach numbers and small surface thickness.

In our case, the interaction between the impeller and the diffuser blades is considered as the main source of noise radiated by the centrifugal fan [149]. It is expressed by a pressure fluctuation on impeller and diffuser blades. It is, then, of a dipolar nature. This study takes into account only sources located at trailing edge of impeller blades and at the leading edge of blades of diffuser. The rotation of the impeller blades is modeled by rotating sources. Impeller blades are not taken into account in the propagation zone. Thus, we place 17 stationary bipolar acoustic sources located at the leading edge of the blades of diffuser and 9 additional rotating impeller sources located at the trailing edge of each impeller blade.

As for FW&H analogy, the source terms introduced in the LEE are constructed from the momentum equations, and defined by:

$$\boldsymbol{S}_{p_i}(x,y,t) = e^{-\frac{\ln(2)}{2}[(x-x_{s_i}(x,y,t))^2+(y-y_{s_i}(x,y,t))^2]} \times p_i(t) \times [0, n_{x_i}, n_{y_i}, 0]^T \tag{60}$$

the subscribe $i$ corresponds to the identification of each blade, the position of the sources is defined by the coordinates $(x_s(x,y,t), y_s(x,y,t))$. For the impeller each source moves following a circle path, the diffuser sources are static. $p_i(t)$ is the aerodynamic static pressure and $(n_x, n_y)$ are the components of the unit radial vector at sources $(x_s, y_s)$. The exponential term of (60) models the punctual nature of the considered sources.

Acoustic pressure history is presented in Fig. 15. At the beginning of the simulation we can observe clearly the position of sources. But soon we lose track of them because of reflections and interference. Thus, all these effects will be explicitly represented in the far field. Note that they are not represented when other approach is used (FW&H, for example).

## 7 Conclusions

In this work we have presented the features of a high-order finite volume method (FV-MLS) and its use for CAA in the context of hybrid approaches. In this approach, we require the computation of the turbulent flow to obtain the acoustic sources. These sources are propagated using an acoustic analogy or the Linearized Euler Equations. After a non-extensive review about different approaches to the computation of turbulent flows and acoustic wave propagation, we have examined the dispersion and dissipation curves of the FV-MLS method, as these properties play a fundamental role in the simulation of wave propagation. Moreover, these properties are also useful in the definition of an implicit filtering that allow us to use the FV-MLS method in a no-model framework for the simulation of turbulent flows. The possibility of using the FV-MLS method for LES calculation in a no-model approach is shown by the computation of the isotropic turbulence decay problem. We have also applied the FV-MLS method to the simulation of acoustic wave propagation in a benchmark case and also in complex geometries using unstructured grids. Obtained results are excellent and they show the real potential of FV-MLS for the simulation of wave-propagation phenomena. From our analysis and numerical results we conclude that the FV-MLS is an effective tool for the simulation of aeroacoustics in complex geometries using unstructured grids.

**Acknowledgements** This work has been partially supported by the *Ministerio de Ciencia e Innovación* (grant #DPI2009-14546-C02-01 and #DPI2010-16496), by R&D projects of the *Xunta de Galicia* (grants #PGDIT09MDS00718PR and #PGDIT09REM005118PR) co-financed with FEDER funds, and the *Universidade da Coruña*.

## References

1. Godunov SK (1959) A finite difference method for the computation of discontinuous solutions of the equations of fluid dynamics. Mat Sb 47(89):271–306
2. Lele SK (1992) Compact finite difference schemes with spectral-like resolution. J Comput Phys 103:16–42
3. Rizzetta DP, Visbal MR, Blaisdell GA (1999) Application of a high-order compact difference scheme to large-eddy and direct numerical simulation. AIAA paper 99-3714
4. Visbal MR, Gaitonde DV (1999) High-order-accurate methods for complex unsteady subsonic flows. AIAA J 37(10):1231–1239
5. Visbal MR, Rizzeta DP (2002) Large-eddy simulation on curvilinear grids using compact differencing and filtering schemes. J Fluids Eng 124:836–847
6. Canuto C, Hussaini MY, Quarteroni A, Zang TA (2007) Spectral methods. Evolution to complex geometries and applications to fluid dynamics. Springer, New York
7. Karniadakis GE, Sherwin SJ (2005) Spectral/hp element methods for computational fluid dynamics, 2nd edn. Oxford University Press, New York
8. Cottrell JA, Hughes TJR, Bazilevs Y (2009) Isogeometric analysis: toward integration of CAD and FEA. Wiley, New York
9. Hughes TJR, Cottrell JA, Bazilevs Y (2005) Isogeometric analysis: CAD, finite elements, NURBS, exact geometry and mesh refinement. Comput Methods Appl Mech Eng 194:4135–4195
10. Piegl L, Tiller W (1997) The NURBS book, 2nd edn. Springer, New York
11. Lipton S, Evans JA, Bazilevs Y, Elguedj T, Hughes TJR (2010) Robustness of isogeometric structural discretizations under severe mesh distortion. Comput Methods Appl Mech Eng 199:357–373
12. Cottrell JA, Reali A, Bazilevs Y, Hughes TJR (2006) Isogeometric analysis of structural vibrations. Comput Methods Appl Mech Eng 195:5257–5296

13. Van Leer B (1979) Towards the ultimate conservative difference scheme V. A second order sequel to Godunov's method. J Comput Phys 32:101–136
14. Van Leer B (1982) Flux vector splitting for the Euler equations. Lecture notes in physics, vol 170. Springer, Berlin
15. Roe PL (1981) Approximate Riemann solvers, parameter vectores and difference schemes. J Comput Phys 43:357–372
16. Venkatakrishnan V (1995) Convergence to steady state solutions of the Euler equations on unstructured grids with limiters. J Comput Phys 118:120–130
17. Barth TJ (1995) Aspects of unstructured grids and finite-volume solvers for the Euler and Navier-Stokes equations. VKI lecture series 1994–95
18. Barth TJ, Frederickson PO (1990) Higher-order solution of the Euler equations on unstructured grids using quadratic reconstruction. AIAA paper 90-0013
19. Barth TJ, Jespersen DC (1989) The design and application of upwind schemes on unstructured meshes. AIAA paper 89-0366
20. Colella P, Woodward P (1984) The piecewise parabolic method (PPM) for gas-dynamical simulations. J Comput Phys 54:174–201
21. Jameson A, Baker TJ (1983) Solution of the Euler equations for complex configurations. AIAA paper 83-1929
22. Frink NT (1992) Upwind scheme for solving the Euler equations on unstructured tetrahedral meshes. AIAA J 30:70
23. Ollivier-Gooch CF, Van Altena M (2002) A high-order accurate unstructured mesh finite volume scheme for the advection-diffusion equation. J Comput Phys 181:729–752
24. Bassi F, Rebay S (1997) A higher-order accurate discontinuous finite element solution of the 2D Euler equations. J Comput Phys 138:251–285
25. Bassi F, Rebay S (1997) A higher-order accurate discontinuous finite element method for the numerical solution of the compressible Navier-Stokes equations. J Comput Phys 131:267–279
26. Bassi F, Rebay S (1997) High-order accurate discontinuous finite element solution of the 2D Euler equations. J Comput Phys 138:251–285
27. Cockburn B, Shu C-W (1998) The local discontinuous Galerkin finite element method for convection-diffusion systems. SIAM J Numer Anal 35:2440–2463
28. Cockburn B, Shu C-W (1989) TVB Runge-Kutta local projection discontinuous Galerkin finite element method for conservation laws II: general framework. Math Comput 52:411–435
29. Cockburn B, Lin SY, Shu C-W (1989) TVB Runge-Kutta local projection discontinuous Galerkin finite element method for conservation laws III: one dimensional systems. J Comput Phys 84:90–113
30. Cockburn B, Hou S, Shu C-W (1990) TVB Runge-Kutta local projection discontinuous Galerkin finite element method for conservation laws IV: the multidimensional case. Math Comput 54:545–581
31. Cockburn B, Shu C-W (1998) The local discontinuous Galerkin method for time-dependent convection-diffusion systems. SIAM J Numer Anal 35:2440–2463
32. Cockburn B, Kanschat G, Perugia I, Schötzau D (2001) Superconvergence of the local discontinuous Galerkin method for elliptic problems on Cartesian grids. SIAM J Numer Anal 39(1):264–285
33. Cockburn B, Shu C-W (2001) Runge-Kutta discontinuous Galerkin methods for convection dominated problems. J Sci Comput 16:173–261
34. Crivellini A, Bassi F (2003) A three-dimensional parallel discontinuous Galerkin solver for acoustic propagation studies. International Journal of aeroacoustics 2:157–174
35. Dolejší V (2004) On the discontinuous Galerkin method for the numerical solution of the Navier-Stokes equations. Int J Numer Methods Fluids 45:1083–1106
36. Zhang M, Shu C-W (2003) An analysis of three different formulations of the discontinuous Galerkin method for diffusion equations. Math Models Methods Appl Sci 13(3):395–413
37. Peraire J, Persson P-O (2008) The compact discontinuous Galerkin (CDG) method for elliptic problems. SIAM J Sci Comput 30(4):1806–1824
38. Persson P-O, Peraire J (2008) Newton-GMRES preconditioning for discontinuous Galerkin discretizations of the Navier-Stokes equations. SIAM J Sci Comput 30(6):2709–2733
39. Harten A, Osher S (1987) Uniformly high order accurate non-oscillatory schemes I. SIAM J Numer Anal 24:279–309
40. Harten A, Engquist B, Osher S, Chakravarthy S (1987) Uniformly high order essentially non-oscillatory schemes III. J Comput Phys 71:231–303
41. Hu CQ, Shu CW (1999) Weighted essentially non-oscillatory schemes on triangular meshes. J Comput Phys 150:97–127
42. Shu CW, Osher S (1988) Efficient implementation of essentially non-oscillatory shock-capturing schemes. J Comput Phys 77:439–471
43. Shu CW, Osher S (1989) Efficient implementation of essentially non-oscillatory shock-capturing schemes II. J Comput Phys 83:32–78
44. Shu CW (1997) Essentially non-oscillatory and weighted essentially non-oscillatory schemes for hyperbolic conservation laws. ICASE Report 97-65
45. Shu CW, Osher S (1989) Efficient implementation of essentially non-oscillatory shock-capturing schemes II. J Comput Phys 83:32–78
46. Abgrall R (1994) On essentially non-oscillatory schemes on unstructured meshes: analysis and implementation. J Comput Phys 114:45–58
47. Borges R, Carmona M, Costa B, Don WS (2008) An improved weighted essentially non-oscillatory scheme for hyperbolic conservation laws. J Comput Phys 227(6):3101–3211
48. Capdeville G (2008) A central WENO scheme for solving hyperbolic conservation laws on non-uniform meshes. J Comput Phys 227:2977–3014
49. Dumbser M, Käser M (2007) Arbitrary high order non-oscillatory finite volume schemes on unstructured meshes for linear hyperbolic systems. J Comput Phys 221:693–723
50. Dumbser M, Käser M, Titarev VA, Toro EF (2007) Quadrature-free non-oscillatory finite volume schemes on unstructured meshes for nonlinear hyperbolic systems. J Comput Phys 226:204–243
51. Henrick AK, Aslam TD, Powers JM (2005) Mapped weighted essentially non-oscillatory schemes: achieving optimal order near critical points. J Comput Phys 207:542–567
52. Sonar T (1997) On the construction of essentially non-oscillatory finite volume approximations to hyperbolic conservation laws on general triangulations: polynomial recovery, accuracy and stencil selection. Comput Methods Appl Mech Eng 140:157–181
53. Zhang YT, Shu CW (2009) Third order WENO scheme on three dimensional tetrahedral meshes. Commun Comput Phys 5:836–848
54. Wang ZJ (2002) Spectral (finite) volume method for conservation laws on unstructured grids. Basic formulation. J Comput Phys 178:210–251
55. Wang ZJ, Liu Y (2002) Spectral (finite) volume method for conservation laws on unstructured grids II: extension to two-dimensional scalar equation. J Comput Phys 179:665–697
56. Wang ZJ, Liu Y (2004) Spectral (finite) volume method for conservation laws on unstructured grids III: one-dimensional systems and partition optimization. J Sci Comput 20:137–157
57. Wang ZJ, Liu Y (2004) Spectral (finite) volume method for conservation laws on unstructured grids IV: extension to two-dimensional systems. J Comput Phys 194:716–741

58. Liu Y, Vinokurb M, Wang ZJ (2006) Spectral (finite) volume method for conservation laws on unstructured grids V: extension to three-dimensional systems. J Comput Phys 212(2):454–472
59. Wang ZJ, Liu Y (2006) Spectral (finite) volume method for conservation laws on unstructured grids VI: extension to viscous flow. J Comput Phys 215:41–58
60. Kannan R, Wang ZJ (2009) A study of viscous flux formulations for a p-multigrid spectral volume Navier Stokes solver. J Sci Comput 41(2):165–199
61. Roe PL (1982) Fluctuations and signals—a framework for numerical evolution problems. In: Morton KW, Baines MJ (eds) Numerical methods for fluid dynamics. Academic Press, San Diego, pp 219–257
62. Roe PL (1987) Linear advection schemes on triangular meshes. Cranfield Institute of Technology, Report 8720
63. Roe PL (1994–1995) Multidimensional upwinding. Motivation and concepts. VKI lecture series
64. Deconinck H, Paillère H, Struijs R, Roe PL (1993) Multidimensional upwind schemes based on fluctuation-splitting for systems of conservation laws. Comput Mech 11:323–340
65. Paillère H, Boxho J, Degrez G, Deconinck H (1996) Multidimensional upwind residual distribution schemes for the convection-diffusion equation. Int J Numer Methods Fluids 23:923–936
66. Issman E, Degrez G, Deconinck H (1996) Implicit upwind residual-distribution Euler and Navier-Stokes solver on unstructured meshes. AIAA J 34(10):2021–2028
67. Hubbard ME, Roe PL (2000) Compact high-resolution algorithms for time-dependent advection on unstructured grids. Int J Numer Methods Fluids 33(5):711–736
68. Deconinck H, Sermeus K, Abgrall R (2000) Status of multidimensional upwind residual distribution schemes and applications in aeronautics. AIAA paper 2000–2328
69. Abgrall R (2001) Toward the ultimate conservative scheme: following the quest. J Comput Phys 167:277–315
70. Abgrall R, Roe PL (2003) Construction of very high order fluctuation schemes. J Sci Comput 19:3–36
71. Abgrall R, Mezine M (2003) Construction of second order accurate monotone and stable residual distribution schemes for unsteady flow problems. J Comput Phys 188:16–55
72. Abgrall R, Mezine M (2004) Construction of second order accurate monotone and stable residual distribution schemes for steady problems. J Comput Phys 195:474–507
73. Abgrall R, Barth TJ (2002) Weighted residual distribution schemes for conservation laws via adaptive quadrature. SIAM J Sci Comput 24:732–769
74. Abgrall R (2006) Essentially non-oscillatory residual distribution schemes for hyperbolic problems. J Comput Phys 214:773–808
75. Abgrall R, Roe PL (2003) High order fluctuation schemes on triangular meshes. J Sci Comput 19:3–36
76. Abgrall R, Adrianov N, Mezine M (2005) Towards very high-order accurate schemes for unsteady convection problems on unstructured meshes. Int J Numer Methods Fluids 47:679–691
77. Ricchiuto M, Csìk Á, Deconinck H (2005) Residual distribution for general time dependent conservation laws. J Comput Phys 209:249–289 2005
78. De Palma P, Pascazio G, Rubino DT, Napolitano M (2006) Multidimensional upwind residual distribution schemes for the convection-diffusion equation. J Comput Phys 218:159–199
79. Abgrall R, Marpeau F (2007) Residual distribution schemes on quadrilateral meshes. J Sci Comput 30:131–175
80. Cueto-Felgueroso L, Colominas I, Fe J, Navarrina F, Casteleiro M (2006) High order finite volume schemes on unstructured grids using moving least squares reconstruction. Application to shallow waters dynamics. Int J Numer Methods Eng 65:295–331
81. Cueto-Felgueroso L, Colominas I, Nogueira X, Navarrina F, Casteleiro M (2007) Finite volume solvers and moving least-squares approximations for the compressible Navier-Stokes equations on unstructured grids. Comput Methods Appl Mech Eng 196:4712–4736
82. Lancaster P, Salkauskas K (1981) Surfaces generated by moving least squares methods. Math Comput 37(155):141–158
83. Liu WK, Li S, Belytschko T (1997) Moving least square reproducing kernel method part I: methodology and convergence. Comput Methods Appl Mech Eng 143:113–154
84. Liu WK, Hao W, Chen Y, Jun S, Gosz J (1997) Multiresolution reproducing kernel particle methods. Comput Mech 20:295–309
85. Nogueira X, Cueto-Felgueroso L, Colominas I, Gómez H, Navarrina F, Casteleiro M (2009) On the accuracy of finite volume and discontinuous Galerkin discretizations for compressible flow on unstructured grids. Int J Numer Methods Eng 78:1553–1584
86. Cueto-Felgueroso L, Colominas I (2008) High-order finite volume methods and multiresolution reproducing kernels. Arch Comput Methods Eng 15(2):185–228
87. Nogueira X, Cueto-Felgueroso L, Colominas I, Navarrina F, Casteleiro M (2010) A new shock-capturing technique based on moving least squares for higher-order numerical schemes on unstructured grids. Comput Methods Appl Mech Eng 199(37–40):2544–2558
88. George WK (2005) Lectures in turbulence for the 21st century. Department of Thermo and Fluid Engineering, Chalmers University of Technology, Göteborg, Sweden
89. Sagaut P (2005) Large eddy simulation for incompressible flows. An introduction, 3rd edn. Springer, Berlin
90. Garnier E, Adams N, Sagaut P (2009) Large-eddy simulation for compressible flows. Scientific computation series. Springer, Berlin
91. Pope SB (2000) Turbulent flows. Cambridge University Press, Cambridge
92. Wilcox DC (1994) Turbulence modelling for CFD. DCW industries
93. Richardson LF (1922) Weather prediction by numerical process. Cambridge University Press, Cambridge (republished by Dover in 1965)
94. Kolmogorov AN (1941) The local structure of turbulence in incompressible viscous fluid for very large Reynolds numbers. Dokl Akad Nauk SSSR 30:301–305 (in Russian), translated to English in Kolmogorov AN (1991) in The local structure of turbulence in incompressible viscous fluid for very large Reynolds numbers, Proceedings of the Royal Society of London, Series A: mathematical and physical sciences 434(1890):9–13
95. Davidson PA (2004) Turbulence. An introduction for scientist and engineers. Oxford University Press, London
96. Orszag SA, Patterson GS (1972) Numerical simulation of turbulence. In: Lecture notes in physics, vol 12. Springer, London, pp 127–147
97. Kolmogorov AN (1942) Equations of turbulent motion of an incompressible flow. Izv Akad Nauk Uzbekskoi SSR Ser Fizico-Mat Nauk 6:56–58 (in Russian), A translation is found in Spalding, DB, Kolmogorov's two-equation model of turbulence, Proc Math Physical Sci, 434(1890):211–216. Turbulence and stochastic process: Kolmogorov's ideas 50 years on 1991
98. Launder BE, Sharma BI (1974) Application of the energy dissipation model of turbulence to the calculation of flow near a spinning disc. Lett Heat Mass Transf 1:131–138
99. Spalding DB (1991) Kolmogorov's two-equation model of turbulence. Proc Math Phys Sci 434(1890):211–216. Turbulence and stochastic process: Kolmogorov's ideas 50 years
100. Menter FR (1993) Zonal two equation $k-\omega$ turbulence models for aerodynamic flows. AIAA paper 93-2906
101. Lien FS, Durbin PA (1996) Non-linear $k-\epsilon-\overline{\nu^2}$ modeling with application to high-lift. CTR summer proceedings

102. Barenblatt GI (1996) Scaling, self-similarity, and intermediate asymptotics. Cambridge University Press, Cambridge
103. Yakhot V, Orszag SA (1986) Renormalization group analysis of turbulence. J Sci Comput 1(1):3–51
104. Liou WW (1991) Modeling of compressible turbulent shear flows. NASA technical report 19920014097
105. Lele SK (1994) Compressibility effect on turbulence. Annu Rev Fluid Mech 26:211–254
106. Lele SK (1993) Notes on the effect of compressibility on turbulence. Center for turbulence research manuscripts, 145, Standford University
107. Batchelor GK (1953) The theory of homogeneous turbulence. Cambridge University Press, Cambridge
108. Kovasznay LSG (1953) Turbulence in supersonic flow. J Aeronaut Sci 20(10):657–682. Reprinted in the AIAA J Spec Suppl: Centennial of powered flight: a retrospective of aerospace research, GM Faeth, Library of flight series, vol 41, 2003
109. Pope SB (1975) A more general effective-viscosity hypothesis. J Fluid Mech 72:331–340
110. Yoshizawa A (1984) Statistical analysis of the derivation of the Reynolds stress from its eddy-viscosity representation. Phys Fluids 27:1377–1387
111. Rubinstein R, Barton JM (1990) Nonlinear Reynolds stress models and the renormalization group. Phys Fluids A 2:1472–1476
112. Deardorff JW (1970) A numerical study of three-dimensional turbulent channel flow at large Reynolds numbers. J Fluid Mech 41(2):453–480
113. Ferziger JH (1976) Large eddy numerical simulations of turbulent flows. AIAA paper 76-347. San Diego, CA
114. Wagner GJ, Liu WK (2000) Turbulence simulation and multiple scale subgrid models. Comput Mech 25:117–136
115. Haselbacher A, Vasilyev OV (2003) Commutative discrete filtering on unstructured grids based on least-squares techniques. J Comput Phys 187:197–211
116. Marsden AL, Vasilyev OV, Moin P (2002) Construction of commutative filters for LES on unstructured meshes. J Comput Phys 175:584–602
117. Stolz S (2005) High-pass filtered eddy-viscosity models for large-eddy simulations of compressible wall-bounded flows. J Fluids Eng 127:666–673
118. Vreman AW (2003) The filtering analog of the variational multiscale method in large-eddy simulation. Phys Fluids 15(8):L61–L64
119. Vreman B, Geurts B, Kuerten H (1995) A priori tests of large Eddy simulation of the compressible plane mixing layer. J Eng Math 29(4):199–327
120. Smagorinsky J (1963) General circulation experiments with the primitive equations. Mon Weather Rev 91(3):99–164
121. Germano M, Piomelli U, Moin P, Cabot WH (1991) A dynamic subgrid-scale eddy viscosity model. Phys Fluids A 3(7):1760–1765
122. Moin P, Squires K, Cabot WH, Lee S (1991) A dynamic subgrid-scale model for compressible turbulence and scalar transport. Phys Fluids A 3(11):2746–2757
123. Stolz S, Adams NA, Kleiser L (1999) Analysis of sub-grid scales and sub-grid scale modeling for shock-boundary-layer interaction. In: Banerjee S, Eaton J (eds) Turbulence and Shear Flow I. Begell House, New York, pp 881–886
124. Hughes TJR, Mazzei L, Jansen KE (2000) Large-eddy simulation and the variational multiscale method. Comput Vis Sci 3:47–59
125. Hughes TJR, Mazzei L, Oberai AA, Wray AA (2001) The multiscale formulation of large-eddy simulation: decay of homogeneous isotropic turbulence. Phys Fluids 13:505–512
126. Hughes TJR, Oberai AA, Mazzei L (2001) Large-eddy simulation of turbulent channel flows by the variational multiscale method. Phys Fluids 13:1784–1799
127. Hughes TJR, Sangalli G (2007) Variational multiscale analysis: the fine-scale Green's function, projection, optimization, localization and stabilized methods. SIAM J Numer Anal 45:539–557
128. Collis SS (2001) Monitoring unresolved scales in multiscale turbulence modeling. Phys Fluids 13(6):1800–1806
129. Bazilevs Y, Calo VM, Cottrell JA, Hughes TJR, Reali A, Scovazzi G (2007) Variational multiscale residual-based turbulence modeling for large eddy simulation of incompressible flows. Comput Methods Appl Mech Eng 197:173–201
130. Voke PR (1990) Multiple mesh simulation of turbulent flow. Technical report QMW EP-1082. Queen Mary and Westfield College, University of London, UK
131. Terracol M, Sagaut P, Basdevan C (2001) A multilevel algorithm for large-eddy simulation of turbulent compressible flows. J Comput Phys 167(2):439–474
132. Sagaut P, Labourasse E, Quémére P, Terracol M (2000) Multiscale approaches for unsteady simulation of turbulent flows. Int J Nonlinear Sci Numer Simul 1(4):285–298
133. Stolz S, Adams NA (1999) An approximate deconvolution procedure for large-eddy simulation. Phys Fluids 11:1699–1701
134. Stolz S, Schlatter P, Meyer D, Kleiser L (2003) High-pass filtered eddy-viscosity models for LES. In: Friedrich VR, Geurts BJ, Métais O (eds) Direct and large-eddy simulation. Kluwer Academic, Dordrecht, pp 81–88
135. Mathew J (2003) An explicit filtering method for LES of compressible flows. Phys Fluids 15:2279–2289
136. Beaudan P, Moin P (1994) Numerical experiments on the flow past a circular cylinder at sub-critical Reynolds numbers. Dept. of Mechanical Engineering, Rept. TF-62. Stanford University, Stanford, CA
137. Mittal R, Moin P (1997) Suitability of upwind-biased finite difference schemes for large-eddy simulation of turbulent flows. AIAA J 35(8):1415–1417
138. Nogueira X, Cueto-Felgueroso L, Colominas Gómez H (2010) Implicit large eddy simulation of non-wall-bounded turbulent flows based on the multiscale properties of a high-order finite volume method. Comput Methods Appl Mech Eng 199:315–624
139. Boris JP, Grinstein FF, Oran ES, Kolbe RJ (1992) New insights into large eddy simulation. Fluid Dyn Res 10:199–228
140. Oran ES, Boris JP (1993) Computing turbulent shear flows—a convenient conspiracy. Comput Phys 7:523–533
141. Porter DH, Pouquet A, Woodward PR (1994) Kolmogorv-like spectra in decaying three-dimensional supersonic flows. Phys Fluids 6:2133–2142
142. Margolin LG, Smolarkiewicz PK, Sorbjan Z (1999) Large eddy simulations of convective boundary layers using nonoscillatory differencing. Physica D 133:390–397
143. Grinstein FF, Fureby C (2002) Recent progress on MILES for high Reynolds number flows. J Fluids Eng 124:848–861
144. Margolin LG, Rider WJ (2002) A rationale for implicit turbulence modelling. Int J Numer Methods Fluids 39:821–841
145. Porter DH, Pouquet A, Woodward PR (1992) A numerical study of supersonic turbulence. Theor Comput Fluid Dyn 4:13–49
146. Johnsen E et al (2010) Assessment of high-resolution methods for numerical simulations of compressible turbulence with shock waves. J Comput Phys 229(4):1213–1237
147. Maaloum A, Kouidri S, Rey R (2004) Aeroacoustic performances evaluation of axial fans based on the unsteady pressure field on the blades surface. Appl Acoust 65:367–384
148. Moon Young J, Cho Y, Nam H-S (2003) Computation of unsteady viscous flow and aeroacoustic noise of cross flow fans. Comput Fluids 32:995–1015
149. Khelladi S, Kouidri S, Bakir F, Rey R (2008) Predicting tonal noise from a high speed vaned centrifugal fan. J Sound Vib 313(1–2):113–133
150. Farassat F, Myers MK (1988) Extension of Kirchhoff's formula to radiation from moving surfaces. J Sound Vib 123:451–560

151. Colonius T, Lele SK (2004) Computational aeroacoustics: progress on nonlinear problems of sound generation. Prog Aerosp Sci 40:345–416
152. Bogey C, Bailly C, Juvé D (2002) Computation of flow noise using source terms in linearized Euler's equations. AIAA J 40(2):235–243
153. Williams JE, Hawkings DL (1969) Sound generation by turbulence and surfaces in arbitrary motion. Phil Trans R Soc Lond A 264(1151):321–342, doi:10.1098/rsta.1969.0031
154. Moon Young J, Seo Jung H (2006) Linearized perturbed compressible equations for low Mach number aeroacoustics. J Comput Phys 218(2):702–719
155. Lynam EJ, Webb HA (1919) The emission of sound by airscrews. R. & M., No 624
156. Bryan GH (1920) The acoustics of moving sources with application to airscrews. R. & M., No 684, British A.R.C.
157. Gutin L (1936) On the sound field of a rotating propeller NACA TM1195 (Traduction de Über das Schallfeld einer rotierenden Luftschraube. Phys Z Sowjetunion 9(1):57–71
158. Lighthill MJ (1952) On sound generated aerodynamically, I. General theory. Proc R Soc Lond Ser A 211:564–587
159. Lighthill MJ (1954) On sound generated aerodynamically, II. Turbulence as a source of sound. Proc R Soc A 222(1148):1–32, doi:10.1098/rspa.1954.0049
160. Curle N (1955) The influence of solid boundaries upon aerodynamic sound. Proc R Soc Lond Ser A 231:505–514
161. Harten A, Lax P, Van Leer B (1983) On upstream differencing and Godunov-type schemes for hyperbolic conservation laws. SIAM Rev 25:35–61
162. Jahawar P, Kamath H (2000) A high-resolution procedure for Euler and Navier-Stokes computations on unstructured grids. J Comput Phys 164:165–203
163. Barth TJ (1993) Recent developments in high order k-exact reconstruction on unstructured meshes. AIAA paper 93-0068
164. Ollivier-Gooch CF, Nejat A, Michalak K (2007) On obtaining high-order finite volume solutions to the Euler equations on unstructured meshes. In: 18th AIAA computational fluid dynamics conference. AIAA, Washington
165. Dumbser M, Balsara DW, Toro EF, Munz CD (2008) A unified framework for the construction of one-step finite volume and discontinuous Galerkin schemes on unstructured meshes. J Comput Phys 227:8209–8253
166. Dumbser M (2010) Arbitrary high order PNPM schemes on unstructured meshes for the compressible Navier-Stokes equations. Comput Fluids 39(1):60–76
167. Nogueira X, Cueto-Felgueroso L, Colominas, Khelladi S. (2010) On the simulation of wave propagation with a higher-order finite volume scheme based on reproducing kernel methods. Comput Methods Appl Mech Eng 199:1471–1490
168. Khelladi S, Martin S, Nogueira X, Bakir F (2010) Higher-order preserving methods for unsteady finite volume solvers based on reproducing kernels: application to aeroacoustic problems. In: 16th AIAA/CEAS, Aeroacoustics conference, Stockholm, Sweden, AIAA paper 2010-3817
169. Venkatakrishnan V, Mavriplis D (1996) Implicit method for the computation of unsteady flows on unstructured grids. J Comput Phys 127:380–397
170. Bailly C, Bogey C (2006) An overview of numerical methods for acoustic wave propagation. In: Wesseling P, Oñate E, Périaux J (eds) European conference on computational fluid dynamics, ECCOMAS CFD
171. Hardin JC, Ristorcelli JR, Tam CKW (1995) ICASE/LaRC workshop on benchmark problems in computational aeroacoustics. NASA conference publication, vol 3300
172. Viswanathan K, Sankar LN (1995) A comparative study of upwind and MacCormack schemes for CAA benchmark problems. In: ICASE/LaRC workshop on benchmark problems in computational aeroacoustics, pp 185–195
173. Tam CKW, Shen H (1993) Direct computation of nonlinear acoustic pulses using high order finite difference schemes. AIAA paper 93-4325
174. Ducros F, Ferrand V, Nicoud F, Weber C, Darracq D, Gacherieu C, Poinsot T (1999) Large-eddy simulation of the shock/turbulence interaction. J Comput Phys 152:517–549
175. Pirozzoli S (2002) Conservative hybrid compact-WENO schemes for shock-turbulence interaction. J Comput Phys 178:81–117
176. Harten A (1978) The artificial compression method for computation of shocks and contact discontinuities. III. Self adjusting hybrid schemes. Math Comput 32:363–389
177. Adams NA, Shariff K (1996) A high-resolution hybrid compact-ENO scheme for shock-turbulence interaction problems. J Comput Phys 127:27–51
178. Sjögreen B, Yee HC (2004) Multiresolution wavelet based adaptive numerical dissipation control for high order methods. J Sci Comput 20:211–255
179. Spyropoulos ET, Blaisdell GA (1996) Evaluation of the dynamic model for simulations of compressible decaying isotropic turbulence. AIAA J 34(5):990–998
180. Sarkar S, Erlebacher G, Hussaini MY, Kreiss HO (1991) The analysis and modelling of dilatational terms in compressible turbulence. J Fluid Mech 227:473–493
181. Bataille F (1994) Etude d'une turbulence faiblement compressible dans le cadre d'une modelisation Quasi-Normale avec Amortissement Tourbillonaire. Thèse Ecole Central de Lyon
182. Hussaini MY (1998) On large-eddy simulation of compressible flows. AIAA 29th fluid dynamics conference, Albuquerque, New Mexico, Paper AIAA 98-2802
183. Colonius T, Lele SK, Moin P (1993) Boundary conditions for direct computation of aerodynamic sound generation. AIAA J 31(9):1574–1582
184. Hu FQ (1996) On absorbing boundary conditions for linearized Euler equations by a perfectly matched layer. J Comput Phys 129:201–219
185. Tam CKW, Webb JC (1993) Dispersion-relation-preserving finite difference schemes for computational aeroacoustics. J Comput Phys 107:262–281
186. Bernacki M, Lanteri S, Piperno S (2006) Time-domain parallel simulation of heterogeneous wave propagation on unstructured grids using explicit, non-diffusive, discontinuous Galerkin methods. J Comput Acoust 14(1):57–82
187. Nogueira X, Cueto-Felgueroso L, Colominas I, Khelladi S, Navarrina F, Casteleiro M (2010) Resolution of computational aeroacoustics problem on unstructured grids with high-order finite volume scheme. J Comput Appl Math 234(7):2089–2097
188. Bailly C, Juvé D (2000) Numerical solution of acoustic propagation problems using linearized Euler equations. AIAA J 38(1):22–29
189. Khelladi S, Kouidri S, Bakir F, Rey R (2005) Flow study in the impeller-diffuser interface of a vaned centrifugal fan. ASME J Fluids Eng 127:495–502